Agricultural and Forest Meteorology 149 (2009) 2162–2182

Contents lists available at ScienceDirect

Agricultural and Forest Meteorology

journal homepage: www.elsevier.com/locate/agrformet

Intercomparison of a 'bottom-up' and 'top-down' modeling paradigm for estimating carbon and energy fluxes over a variety of vegetative regimes across the U.S.☆

Rasmus Houborg [a,*], Martha C. Anderson [b], John M. Norman [c], Tim Wilson [d], Tilden Meyers [d]

[a] Earth System Science Interdisciplinary Center, University of Maryland, College Park and Hydrological Sciences Branch, NASA Goddard Space Flight Center, Greenbelt, MD, USA
[b] USDA-ARS Hydrology and Remote Sensing Laboratory, Beltsville, MD, USA
[c] Department of Soil Science, University of Wisconsin-Madison, 1525 Observatory Drive, Madison, WI 53706, USA
[d] Atmospheric Turbulence and Diffusion Division/NOAA, P.O. Box 2456, Oak Ridge, TN 37831, USA

ARTICLE INFO

Article history:
Received 25 September 2008
Received in revised form 18 March 2009
Accepted 22 June 2009

Keywords:
CO_2 fluxes
Evapotranspiration
Light-use-efficiency
Leaf photosynthesis
Bottom-up model
Top-down model
Stomatal conductance

ABSTRACT

Biophysical models intended for routine applications at a range of scales should attempt to balance the competing demands of generality and simplicity and be capable of realistically simulating the response of CO_2 and energy fluxes to environmental and physiological forcings. At the same time they must remain computationally inexpensive and sufficiently simple to be effectively parameterized at the scale of application. This study investigates the utility of two modeling strategies for quantifying coupled land surface fluxes of carbon and water, which differ distinctly in their description of CO_2 assimilation processes. 'Bottom-up' models of land–atmosphere carbon exchange are based on detailed mechanistic descriptions of leaf-level photosynthetic processes scaled to the canopy whereas 'top-down' scaling approaches neglect the behavior of individual leaves and consider the canopy response to its environment in bulk. Effective intercomparisons of a light-use-efficiency (LUE)-based model of canopy conductance and a mechanistic model of leaf photosynthesis–stomatal response that employs a 'two-leaf' scaling strategy are facilitated by embedding both canopy sub-models in the Atmosphere–Land Exchange (ALEX) surface energy balance model. Water and carbon flux simulations are evaluated across time scales of hours, days, seasons and years for a variety of natural and agricultural ecosystems, using micrometeorological data from several AmeriFlux sites across the U.S. While both modeling paradigms reproduced observed magnitudes and variances of carbon and water vapor exchange on hourly and daily timescales with acceptable accuracy, the simpler LUE-based model often performed better than the more detailed scaled-leaf model, which has many adjustable species-specific model parameters. Actual light-use efficiencies vary significantly in response to changing environmental conditions and the success of LUE-based modeling frameworks rely on their ability to realistically respond to changes in light environment, atmospheric humidity, CO_2 concentration and a desiccating environment.

1. Introduction

An accurate quantification of energy and carbon fluxes is of great importance for a wide range of ecological, agricultural, and meteorological applications. The modeling of atmosphere–land exchange processes at a range of spatial and temporal scales can improve our understanding of ecosystem functioning. These flux evaluations are also important in the context of climate change for the establishment of regional and global carbon budgets. Additionally, reliable regional assessments of land–surface water and energy fluxes have utility in water resource management, yield forecasting, and numerical weather prediction.

Plant physiological research carried out in the 1980s and early 1990s provided new insights into the biochemical mechanisms controlling the CO_2 assimilation of leaves and how stomata respond to environmental and physiological factors (e.g., Farquhar et al., 1980; Ball et al., 1987; Collatz et al., 1991). Stomata simultaneously regulate the conflicting demands of allowing CO_2 assimilation by leaves and minimizing water loss from the leaves to the environment, and this stomatal conductance has been recognized as a key for assessing carbon and latent heat exchange between vegetated surfaces and the atmosphere.

☆ This article was previously published in 2009, Volume 149, issue 11. For citation purposes please use the original publication details; Houborg, R., Anderson, M.C., Norman, J. M., Wilson, T., Meyers, T., 2009. Intercomparison of a 'bottom-up' and 'top-down' modelling paradigm for estimating carbon and energy fluxes over a variety of vegetative regimes across the U.S. Agric. For. Meteorol. 149(11) 1875–1895.

* Corresponding author.
E-mail address: rasmus.houborg@nasa.gov (R. Houborg).

0168-1923/$ – see front matter © 2009 Elsevier B.V. All rights reserved.
doi:10.1016/j.agrformet.2009.10.002

The predictive power of biophysical models has been significantly enhanced by coupling fluxes of carbon dioxide and water vapor using semi-empirical models of stomatal functioning (e.g., Wang and Leuning, 1998; Anderson et al., 2000; Kellomaki and Wang, 2000; Sellers et al., 1996; Zhan and Kustas, 2001; Baldocchi and Wilson, 2001; Anderson et al., 2008).

Biophysical models intended for routine applications at regional scales should be capable of realistically simulating the response of canopy-scale CO_2 and energy fluxes to environmental and physiological forcings but should also remain computationally inexpensive and be sufficiently simple to be effectively parameterized at the scale of application. Very complex modeling systems may require land–surface parameters that cannot be defined with adequate accuracy over large spatial domains.

Two contrasting modeling strategies are currently used widely to quantify canopy-scale exchange processes of CO_2 and water vapor at local, regional and global scales. 'Bottom-up' models of land–atmosphere CO_2 and energy exchange are based on detailed mechanistic descriptions of leaf-level photosynthetic processes scaled to the canopy, whereas 'top-down' scaling approaches neglect the behavior of individual leaves and consider the canopy response to its environment in bulk. 'Bottom-up' models of coupled CO_2–water vapor exchange rely on the specification of an appropriate leaf-to-canopy scaling framework. Big-leaf models that treat the canopy as a single leaf have been used extensively to parameterize land–surface in climate models (e.g., Sellers et al., 1996; Dickenson et al., 1998) but have been shown to introduce significant errors into calculations of canopy photosynthesis (De Pury and Farquhar, 1997; Spitters, 1986). Multi-layer integration schemes (e.g., Leuning et al., 1995; Baldocchi and Wilson, 2001) consider multiple layers with many different leaf angle classes and numerically integrate fluxes for each leaf class and layer to derive total canopy fluxes. The complexity and high computational demand is an evident drawback of the multi-layer approach. The two-leaf concept represents a simplified canopy integration scheme that largely overcomes the limitations of 'big-leaf' models as it considers the highly non-linear response of leaf photosynthesis to the different light environments of sunlit and shaded leaves (De Pury and Farquhar, 1997; Wang and Leuning, 1998). 'Bottom-up' (scaled-leaf) models generally require the specification of many species-dependent leaf-scale parameters but have proven effective in reproducing observed fluxes at a range of scales (Leuning et al., 1998; Houborg and Soegaard, 2004; Zhan and Kustas, 2001; Dai et al., 2004).

'Top-down' models are generally less complex, as they are constrained by some empirical relationship developed at the stand-level and thus implicitly incorporate scaling effects. The light-use-efficiency (LUE), defined here as the ratio between net CO_2 assimilation rate and absorbed photosynthetically active radiation (APAR), is a fundamental quantity used by a suite of simple biophysical models (e.g., Ruimy et al., 1994; Prince and Goward, 1995; Potter et al., 2003; Running and Hunt, 1993) that assume conservation of LUE for major vegetation types under unstressed conditions. Models constrained by LUE generally require the specification of only few tunable parameters. However due to the embedded empiricism LUE-based models may need modification in order to respond realistically to climate changes such as elevated CO_2 (Harley et al., 1992).

The objective of this study is to compare a simple analytical LUE-based model of canopy resistance with a mechanistic model of leaf-level photosynthesis–stomatal response that employs a 'two-leaf' scaling strategy. The two modeling paradigms differ considerably in their scaling approach and complexity, and a key objective is to test the potential utility of the contrasting modeling paradigms for regional to continental-scale CO_2 and water vapor flux modeling. Effective model evaluations are facilitated by setting up the models using parameterizations for broad categories of vegetation environments as reported in the ecological literature. The study also aims at providing insight into the challenges of model parameterization for the two types of canopy models and may act as a guideline for the degree of model simplicity required for useful flux predictions at larger scales on a routine basis. For the purpose of intercomparisons, both canopy sub-models have been embedded in the Atmosphere–Land Exchange (ALEX) surface energy balance model, which is a simplified version of a detailed soil–plant–atmosphere model Cupid (Norman, 1979; Norman and Campbell, 1983; Norman and Polley, 1989; Norman and Arkebauer, 1991); ALEX was specifically developed for operational applications. The ability of the two canopy sub-models to reproduce observed patterns in energy and carbon fluxes across time scales of hours, days, seasons and years is evaluated for a variety of natural and agricultural ecosystems, using micrometeorological data from several AmeriFlux sites across the U.S.

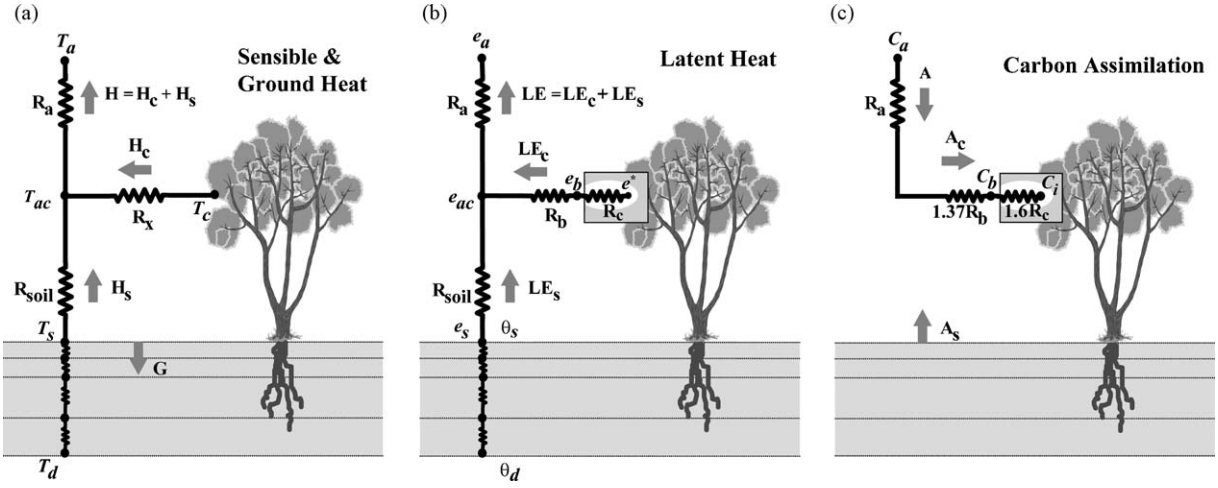

Fig. 1. Transport resistance networks used in the ALEX model to estimate fluxes of (a) sensible (H) and ground heating (G), (b) latent heating from the insides of leaf stomates (LE_c) and the soil surface (LE_s), and (c) net ecosystem CO_2 exchange (A). The subscripts 'a', 'ac', 'b', and 'i' refer, respectively, to conditions above the canopy, within the canopy air space, within the boundary layer at the leaf surface, and inside sub-stomatal cavities. R_a is the aerodynamic resistance to turbulent transport between the canopy air space and measurement reference height, R_b is the resistance of the leaf boundary layer, R_c is the stomatal resistance to water vapor diffusion, and R_{soil} is the aerodynamic resistance of the boundary layer between the soil surface and the canopy air space. The 1.6 and 1.37 resistance multipliers (c) account for the difference in diffusivity between CO_2 and water vapor.

2. Canopy-scale model of atmosphere–and exchange (ALEX)

At the core of the prognostic canopy-scale model of ALEX is a two-layer (soil and vegetation) land–surface representation coupling fluxes from the soil, plants, and atmosphere. The ALEX model has been described in detail in Anderson et al. (2000) and is only briefly summarized here. The conceptual structure of the ALEX model is given in Fig. 1 where the directions of fluxes represent daytime conditions. The latent heat flux at the measurement reference height (LE) represents water vapor evaporation from the insides of leaf stomates (LE_c) and the soil surface (LE_s), H is sensible heat transferred from the canopy air space due to sensible heat convection or conduction from leaf (H_c) and soil surface (H_s), and A is the net ecosystem CO_2 exchange, which incorporates the assimilation of CO_2 inside plant leaves through the stomates minus leaf respiration (A_c) and respiratory loss of CO_2 from soil and roots (A_s). In ALEX, these fluxes are regulated by series-parallel resistance networks that allow both soil and canopy components of the system to modify the in-canopy air temperature and vapor pressure. In Fig. 1, R_a is the aerodynamic resistance to turbulent transport between the canopy air space and measurement reference height, R_b is the resistance of the quasi-laminar sub-layer that forms around a leaf (i.e., the leaf boundary layer), R_c is the stomatal resistance to water vapor diffusion, and R_{soil} is the aerodynamic resistance of the boundary layer between the soil surface and the canopy air space.

For the purpose of this study, two alternative sub-models for estimating canopy fluxes of water and CO_2 were embedded in ALEX. Both sub-models couple fluxes of CO_2 and water vapor using a semi-empirical model of stomatal functioning but they differ distinctly in their description of CO_2 assimilation processes. The 'bottom-up' (scaled-leaf) canopy sub-model is constructed from mechanistic representations of leaf-level photosynthetic processes scaled to the canopy level, whereas the 'top-down' scaling approach of the LUE-based sub-model considers the canopy response to its environment in bulk, neglecting the behavior of individual leaves. Both models incorporate an empirical stress function (Norman, 1979; Campbell and Norman, 1998) that relates depletion of plant available water in the root zone (*faw*) to reductions in transpiration/assimilation due to stomatal closure. The two canopy sub-models are detailed in the next two sections.

In ALEX, the soil heat flux (G) and soil evaporation rate are predicted by a multi-layered (15 layers used here) numerical soil model that serves as the lower boundary of the transport processes above ground. This soil transport module is a generalization of algorithms from Campbell (1985), adapted to a soil structure with layered hydraulic and thermal properties. Profiles of soil temperature (T_s) and water content are updated by solving systems of second-order, time-dependent differential equations using a Newton–Raphson finite-difference solution technique. In the current setup, a single soil texture with uniform hydraulic and thermal properties throughout the profile was assumed for simplicity.

2.1. Scaled-leaf canopy sub-model ('bottom-up')

In the scaled-leaf model, canopy photosynthesis is modeled by applying mechanistic equations of photosynthesis–stomatal response defined at the leaf-scale, where the leaves are separated into sunlit and shaded fractions to facilitate scaling from leaf-to-canopy. The model employs the biochemical equations of leaf photosynthesis by Farquhar et al. (1980), Collatz et al. (1991), and Collatz et al. (1992) as well as the semi-empirical model of stomatal functioning (Ball et al., 1987) to couple CO_2 assimilation and stomatal conductance. The equations of the coupled CO_2 assimilation, stomatal conductance and latent heat flux models are summarized in Table A.1 (Appendix A).

Within the leaf-scale model, leaf-level photosynthesis for C_3 and C_4 photosynthetic pathways is estimated as the minimum of the Rubisco limited rate of ribulose bisphosphate (RuBP) carboxylation (Eq. (A.2)), the electron transport limited (light limited) rate of RuBP regeneration (Eq. (A.3)), and the Carbon compound export limited (C_3) or PEP-carboxylase limited (C_4) rate (Eq. (A.4)) minus leaf respiration (R_d). The rate of CO_2 assimilation for C_3 and C_4 plants is solved from nested quadratics (Eq. (A.6)) to allow for a gradual transition and co-limitation between the three capacities.

The strong non-linear variation of photosynthetic model parameters with temperature is described by an Arrhenius function (Eq. (A.12)). A deactivation function (Eq. (A.14)) was incorporated in the temperature response functions for the maximum Rubisco capacity (V_m) and the Potential rate of electron transport (J_m) to simulate a drop in activity at extreme temperatures. The system of equations describing leaf photosynthesis and stomatal conductance (Eqs. (A.1)–(A.10)) are solved separately for C_3 and C_4 vegetation using cubic analytical solutions (Baldocchi, 1994; Collatz et al., 1992) to avoid the tendency of iterative solutions techniques to arrive at chaotic solutions under specific extreme conditions (Baldocchi, 1994). The resultant stomatal conductance is then used as input to the latent heat flux equation (Eq. (A.11)).

Total canopy photosynthesis and transpiration are calculated as the sum of contributions from sunlit and shaded canopy fractions. This 'two-leaf' scaling strategy is generally assumed to be more reliable than 'big-leaf' models that treat the canopy as a single leaf, due to the highly non-linear response of leaf photosynthesis to the level of irradiance and distinctly different light environments of sunlit and shaded leaves (De Pury and Farquhar, 1997; Wang and Leuning, 1998). The leaf-to-canopy scaling principles adopted here assume that (1) the maximum Rubisco capacity is linearly related to leaf nitrogen and that nitrogen allocation decline exponentially from the top of the canopy (De Pury and Farquhar, 1997; Wang and Leuning, 1998), and (2) the vertical profile of the potential rate of electron transport parallels that of light (Wang and Leuning, 1998). These upscaling equations were modified to consider the clumping effect (Eqs. (A.15)–(A.19)). APAR is partitioned into sunlit and shaded canopy fractions according to De Pury and Farquhar (1997) by considering direct-beam, diffuse and scattered-beam irradiance whereas the partitioning of the canopy net radiation into sunlit and shaded canopy fractions follows Zhan and Kustas (2001).

2.2. LUE-based canopy sub-model ('top-down')

The equations describing the LUE-based sub-model are given in Anderson et al. (2000) and summarized in Table B.1 (Appendix B) to facilitate a direct comparison with the scaled-leaf sub-model. Nominal stand-level measurements of LUE (β_n) and nominal estimates of the ratio of intercellular to ambient CO_2 concentration (γ_n) replace the mechanistic leaf-level photosynthetic equations (Eqs. (A.1)–(A.8)). Since CO_2 assimilation scaling effects are implicitly incorporated into the measurement of β_n, the leaf-to-canopy scaling equations (Eqs. (A.15)–(A.19)) are also avoided. This modeling paradigm exploits the conservative quality of canopy LUE that is observed over seasonal to annual timescales within broad vegetation categories under unstressed environmental conditions (Anderson et al., 2000; Gower et al., 1999). Deviations of the canopy LUE from this nominal value on shorter timescales are accommodated by diagnosing an effective LUE (β) that responds linearly to changes in the ratio of intercellular to ambient CO_2 concentration ($\gamma = C_i/C_a$) (Eq. (B.7)) and the fraction of diffuse radiation (Eq. (B.8)). The model paradigm assumes that under optimal conditions the canopy will tend to operate near β_n with a nominal value of γ (γ_n). An increase in the stomatal resistance in response to e.g., a desiccating environment will

decrease the average C_i and move the canopy toward a lower value of LUE. CO_2 assimilation is linked to canopy stomatal conductance using the approach of Ball et al. (1987) (Eq. (B.4)) and the canopy stomatal resistance is derived using a second-order analytical expression (see Eq. (11) in Anderson et al., 2000), semi-constrained by β_n and γ_n averaged over broad vegetation categories. The modeled canopy stomatal resistance responds to changes in soil moisture availability and variation of environmental conditions of humidity, temperature (ambient and leaf), wind speed, CO_2 concentration, and direct-beam vs. diffuse light composition.

3. Flux tower datasets

Eddy-covariance measurements of surface heat, water and carbon dioxide fluxes were obtained from seven NOAA-ATDD GEWEX (Global Energy and Water Cycle Experiment) air SURFace eXchange (SURFX) sites (http://www.atdd.noaa.gov/gewex.htm) located in diverse land vegetation environments, including grassland (AG, FP, GC), cropland (BV, BP), and forested sites (BH, WB) (Table 1). These sites are also included as a part of the AmeriFlux network (http://public.ornl.gov/ameriflux/) and the measurements and instrumentation follow the AmeriFlux protocol (Baldocchi, 2003).

Net ecosystem CO_2 exchange is the sum of the CO_2 flux densities measured by the eddy-covariance systems and a CO_2 storage term that accounts for CO_2 stored in the layer of air below the eddy-covariance system. CO_2 flux storage may be significant for forest ecosystems especially at night when the atmosphere is stable and winds are calm (Wofsy et al., 1993). CO_2 flux densities without storage correction may show spikes in CO_2 assimilation shortly after sunrise as convective turbulence increases and CO_2 is transported from the canopy into the turbulent boundary layer. The CO_2 flux densities for the two forested sites (WB and BH) were storage corrected using a simple representation of the temporal change in CO_2 concentration at the tower measurement height (Creco and Baldocchi, 1996). CO_2 flux densities measured at the cropland and grassland sites are for the purpose of these intercomparisons assumed representative of the net rate of ecosystem exchange. Carbon taken up by the ecosystem is treated as a positive flux. In terms of energy balance components, heat flux entering the soil volume is positive whereas all other flux densities (mass and energy fluxes) are defined as positive away from the surface. Strict acceptance/rejectance criteria were applied to the flux measurements and the flux records used to validate the models were not gap-filled.

A correction factor was applied to measurements of the soil heat flux obtained at a depth of 4 cm to account for the heat storage in the soil layer above the heat flux plate. The correction was done as described in Mayocchi and Bristow (1995) and considers the time rate of change in soil temperature above the plate and the volumetric heat capacity that varies as a function of soil bulk density, soil texture, organic matter content and soil water content.

The sum of the sensible and latent heat fluxes measured by eddy-covariance is generally less than the available energy measured at the land-surface (the difference between net radiation and soil heat fluxes), and this lack of closure of the surface energy balance has been shown to be on the order of 10–40% of measured net radiation (e.g., Twine et al., 2000; Wilson et al., 2002). In this study, energy balance closure was enforced by modifying the observed sensible and latent heat fluxes such that they summed to the available energy yet retained the observed Bowen ratio (Twine et al., 2000).

Ancillary site observations of incoming solar radiation, longwave incoming radiation, relative humidity, air temperature, atmospheric pressure, precipitation and leaf area index were used as input to the ALEX model. At each site, the seasonal leaf area index data have been estimated as an exponential function of the NDVI derived from 30-min measurements of above-canopy global solar radiation and incoming and outgoing photosynthetically active radiation fluxes (Wilson and Meyers, 2007). Descriptive landcover classes were assigned to each flux tower site based on the University of Maryland (UMD) 1-km global landcover product (Hansen et al., 2000). General site details are given in Table 1. Detailed site descriptions are provided in Wilson and Meyers (2007).

4. Model setup

A complete list of soil, leaf and canopy parameter values used in the ALEX simulations are given in Table 2. The parameters are listed for each of the vegetation environments associated with the flux tower sites and were determined based on nominal data reported in the ecological literature. The parameterizations are intended to be representative of broad categories of vegetation environments and to act as a guideline for model implementations at regional to continental scales.

Table 1
List of flux tower sites, study period and site characteristics including site elevation and tower height, vegetation and soil types and climatic conditions.

Site	ID	Latitude longitude	Study period	Elevation tower h (m)	Landcover class	Soil type	Precip [mm]	Mean T_a [°C]
Audubon Ranch	AG	31°35′27″N 110°30′37″W	January–December (2003–2006)	1469 4	Semi-arid grassland	Sandy loam	356	15.9
Fort Peck	FP	48°18′28″N 105°06′02″W	May–September (2003–2006)	634 3.5	Temperate grassland	Clay loam	218	17.0
Goodwin Creek	GC	34°15′00″N 89°58′12″W	April–October (2003–2006)	87 4	Temperate grassland	Silt loam	636	22.3
Bondville	BV	40°00′22″N 88°17′24″W	May–September (2003–2006)	219 10	Cropland	Silt loam	415	20.6
Bondville companion	BP	40°00′33″N 88°17′26″W	May–September (2004–2005)	219 10	Cropland	Silt loam	415	21.1
Black Hills	BH	44°09′29″N 103°39′00″W	May–October (2003–2006)	1718 24	Evergreen needle-leaf	Clay loam	388	13.2
Walker Branch	WB	35°57′32″N 84°17′15″W	April–October (2003–2006)	343 33	Deciduous broadleaf	Silty clay loam	708	18.6

Table 2
A complete list of soil, leaf and canopy input quantities and values used in the ALEX simulations. Where two values are given (e.g., 0.02/0.03) the values apply to the fraction of plants with C_3 and C_4 pathway, respectively.

Quantity	ID	Units	AG	FP	GC	BV (corn)	BP (soybean)	BH	WB
Shared canopy parameters and variables									
Ambient CO_2 concentration	C_a	μmol mol^{-1}	360	360	360	360	360	360	360
Leaf area index	L	m m^{-1}	0.2–1.1	0.1–4.7	0.1–3.8	0.1–5.1	0.1–6.1	1.5–4.2	0.5–7.5
Fraction of green vegetation	f_g		1.0	1.0	1.0	0.1–1.0	0.1–1.0	1.0	0.1–1.0
Canopy height	h_c	m	0.2	0.1–0.4	0.1–0.4	0–3.0	0–0.9	24	25
Clumping factor at nadir	Ω		0.7	1.0	1.0	0.9	1.0	0.5	0.90
Ratio of canopy width to height	D		1.0	1.0	1.0	1.0	1.0	3.5	1.0
Surface roughness	Z_m	m	$0.16h_c$	$0.05h_c$	$0.05h_c$	$0.1h_c$	$0.1h_c$	$0.1h_c$	$0.1h_c$
Displacement height	d	m	$0.44h_c$	$0.67h_c$	$0.67h_c$	$0.67h_c$	$0.67h_c$	$0.67h_c$	$0.67h_c$
Average leaf size	s	m	0.02	0.02	0.02	0.2	0.03	0.05	0.10
Ball & Berry slope	m		11.0	9.5	9.5	3.5	9.5	9.5	9.5
Ball & Berry offset	b	μmol m^{-2} s^{-1}	0.01×10^6	0.01×10^6	0.01×10^6	0.04×10^6	0.01×10^6	0.01×10^6	0.01×10^6
Minimum RH in Ball & Berry	$RH_{b,min}$		0.6	0.1	0.1	0.1	0.1	0.1	0.1
Stomatal distribution correction factor	f_c		2	2	2	2	2	2	1
Fraction of plants with C_3 pathway	f_{c3}		0.6	0.9	0.6	0.0	1.0	1.0	1.0
Leaf absorptivity (vis) (live)	$a_{l,v}$		0.82	0.82	0.82	0.83	0.83	0.89	0.86
Leaf absorptivity (nir) (live)	$a_{l,n}$		0.28	0.28	0.28	0.35	0.35	0.6	0.37
Leaf absorptivity (vis) (dead)	$a_{d,v}$		0.42	0.42	0.42	0.49	0.49	0.84	0.84
Leaf absorptivity (nir) (dead)	a_{ldn}		0.04	0.04	0.04	0.13	0.13	0.61	0.61
Rooting depth	d_r	m	2.0	2.0	2.0	2.0	2.0	2.0	2.0
Max interception	$W_{i,max}$	mm	0.15	0.15	0.15	0.15	0.15	0.15	0.15
Max fraction of wetted leaf area	$f_{wet,max}$		0.2	0.2	0.2	0.2	0.2	0.2	0.2
LUE module									
Nominal LUE	β_n	mol mol^{-1}	0.02/0.03	0.013/0.03	0.013/0.03	0.040	0.024	0.014	0.020
Nominal C_i/C_a fraction	γ_n	mol mol^{-1}	0.7/0.5	0.7/0.5	0.7/0.5	0.5	0.7	0.7	0.7
C_i/C_a at $\beta = 0$	γ_0	mol mol^{-1}	0.2/0.0	0.2/0.0	0.2/0.0	0.0	0.2	0.2	0.2
Scaled-leaf module									
Maximum Rubisco capacity	V_m^{25}	μmol m^{-2} s^{-1}	122/20	63/20	63/20	30	95	42	53
Leaf respiration	R_d^{25}	μmol m^{-2} s^{-1}	$0.015V_m^{25}$	$0.015V_m^{25}$	$0.015V_m^{25}$	$0.025V_m^{25}$	$0.015V_m^{25}$	$0.015V_m^{25}$	$0.015V_m^{25}$
Nitrogen extinction coefficient	k_n		0.7	0.7	0.7	0.7	0.7	0.5	0.5
Quantum yield for electron transport	α_3	mol mol^{-1}	0.37	0.37	0.37		0.37	0.37	0.37
C4 quantum yield for CO_2 uptake	α_4	mol mol^{-1}	0.062			0.062			
Initial slope of photosynthetic CO_2 esponse	k	mol m^{-2} s^{-1}	$20 \times 10^3 V_m^{25}$			$20 \times 10^3 V_m^{25}$			
Potential rate of electron transport	J_m^{25}	μmol m^{-2} s^{-1}	$1.9V_m^{25}$	$1.9V_m^{25}$	$1.9V_m^{25}$	$1.9V_m^{25}$	$1.9V_m^{25}$	$1.9V_m^{25}$	$1.9V_m^{25}$
Curvature factor	θ_j		0.7	0.7	0.7	0.7	0.7	0.7	0.7
Oxygen partial pressure	O	mmol mol^{-1}	205	205	205	205	205	205	205
Michaelis–Menten constant for CO_2	K_c^{25}	μmol mol^{-1}	404.9	404.9	404.9	404.9	404.9	404.9	404.9
Michaelis–Menten constant for O_2	K_O^{25}	mmol mol^{-1}	278.4	278.4	278.4	278.4	278.4	278.4	278.4
CO_2 compensation point *	Γ^{*25}	μmol mol^{-1}	42.75	42.75	42.75	42.75	42.75	42.75	42.75
Energy of activation for K_O^{25}	$H_{a,1}$	kJ mol^{-1}	79.43	79.43	79.43	79.43	79.43	79.43	79.43
Energy of activation for K_O^{25}	$H_{a,2}$	kJ mol^{-1}	36.38	36.38	36.38	36.38	36.38	36.38	36.38
Energy of activation for Γ^{*25}	$H_{a,3}$	kJ mol^{-1}	37.83	37.83	37.83	37.83	37.83	37.83	37.83
Energy of activation for J_m^{25}	$H_{a,4}$	kJ mol^{-1}	50.00	50.00	50.00	50.00	50.00	50.00	50.00
Energy of activation for V_m^{25}	$H_{a,5}$	kJ mol^{-1}	72.00	72.00	72.00	72.00	72.00	72.00	72.00
Energy of activation for R_d^{25}	$H_{a,6}$	kJ mol^{-1}	46.39	46.39	46.39	46.39	46.39	46.39	46.39
Energy of deactivation for V_m^{25} and J_m^{25}	H_d	kJ mol^{-1}	200.0	200.0	200.0	200.0	200.0	200.0	200.0
Entropy term for V_m^{25}	ΔS_V	kJ mol^{-1} C^{-1}	0.6416	0.649	0.649	0.649	0.649	0.649	0.649
Entropy term for J_m^{25}	ΔS_J	kJ mol^{-1} C^{-1}	0.6410	0.646	0.646	0.646	0.646	0.646	0.646
C_3 curvature (co-limitation) parameter	θ_3		0.92	0.92	0.92	0.92	0.92	0.92	0.92
C_3 curvature (co-limitation) parameter	β_3		0.99	0.99	0.99	0.99	0.99	0.99	0.99
C4 curvature (co-limitation) parameter	θ_4		0.83	0.83	0.83	0.83	0.83	0.83	0.83
C4 curvature (co-limitation) parameter	β_4		0.93	0.93	0.93	0.93	0.93	0.93	0.93
Soil transport module									
Bulk density	BD	g cm^{-3}	1.4	1.32	1.4	1.4	1.4	1.32	1.26
Moisture release parameter	b_s		3.1	5.2	4.7	4.7	4.7	5.2	6.6
Air entry potential	ψ_e	J kg^{-1}	−1.5	−2.6	−2.1	−2.1	−2.1	−2.6	−3.3
Sat. hydraulic conductivity	K_s	kg s m^{-3}	7.2×10^{-4}	6.4×10^{-5}	1.9×10^{-4}	1.9×10^{-4}	1.9×10^{-4}	6.4×10^{-5}	4.2×10^{-5}
Deep soil temperature	T_d	°C	20	12	21	15	15	13	15
Soil emissivity	ε_s		0.96	0.96	0.96	0.96	0.96	0.96	0.96
Soil reflectance (vis)	ρ_{sv}		0.11	0.11	0.11	0.11	0.11	0.08	0.08
Soil reflectance (nir)	ρ_{sn}		0.22	0.22	0.22	0.22	0.22	0.18	0.18

4.1. Shared model parameters and variables

Leaf and soil optical (absorptivities, reflectances, emissivity) properties and leaf sizes were assigned nominal values characteristic of broad landcover classes following Anderson et al. (2007). Surface roughness (Z_m) and displacement height (d) were calculated as landcover dependent fractions of the canopy height (h_c) (Massman, 1997), which is scaled linearly with the fraction of vegetation cover between seasonal minimum and maximum values (Anderson et al., 2007). Forests have been found to exhibit a clumped architecture, and nadir clumping index (Ω) values for several forest ecosystems reported by Gower et al. (1999) and Kuchari et al. (1999) were adopted here. The vegetation heterogeneity at the desert grassland site, characterized by a mixture of grasses and scattered shrubs, was treated by assigning a nadir clumping factor of 0.7. The Ω was assumed to be 0.9 for the C_4

cropland class (Anderson et al., 2007). Randomly distributed leaves were assumed for C_3 cropland as well as the FP and GC grassland sites ($\Omega = 1.0$). The dependence of the clumping index on solar zenith angle was modeled according to Kuchari et al. (1999) by assigning land cover representative values of the ratio between canopy height and nominal clump width (D). The leaf area index (L) record from each site (Section 3) represents green L. At the agricultural and deciduous forest sites, which experienced significant degrees of senescence late in the season, the fraction of green vegetation (f_g) was calculated as green L divided by the average L during the leaf constant period.

The slope and offset of the Ball and Berry stomatal conductance model have been found to be fairly constrained parameters within C_3 and C_4 functional categories for ample soil moisture conditions (e.g., Ball et al., 1987; Leuning, 1990; Collatz et al., 1991). Values between 9 and 10 for the stomatal slope (m) are generally assumed to be appropriate for C_3 vegetation in the mid-latitudes whereas C_4 plants are assigned a value between 3 and 4 (Sellers et al., 1996; Collatz et al., 1992; Kosugi et al., 2003). The steeper stomatal slope ($m = 11$) of the desert grassland site is in accordance with findings reported in Zhan and Kustas (2001) and Gutschick (1996).

A parameter describing the relative distribution of leaves with C_3 and C_4 pathways (f_{c3}) was introduced to allow mixed C_3 and C_4 canopies to be simulated. This was achieved by cycling through the LUE or scaled-leaf canopy subroutine twice using canopy parameters specific to each physiological type in each run. Total canopy estimates were then derived by weighing C_3 and C_4-specific CO_2 and energy fluxes, stomatal conductances and canopy temperatures against the relative distribution of each component within the canopy.

In the soil transport module, soil hydraulic and thermal properties were derived from tabular values in Campbell and Norman (1998) based on the assigned soil texture class (Table 1). A 10 cm thick residual litter layer was simulated at the forested sites by adding a soil layer with hydraulic and thermal properties characteristic of organic material (Lawrence and Slater, 2008). The deep soil temperature (T_d) was estimated for each flux tower site as the average of the observed 100 cm soil temperature during the growing season. The soil moisture profile was initialized with observations made at the flux tower sites.

4.2. LUE-based canopy sub-model

The nominal LUE (β_n) is a key input to the LUE-based canopy sub-model. The β_n is defined as a diffuse beam fraction of 50% (Eq. (B.8)) and it represents conditions when the environment does not constrain photosynthesis as limiting environmental factors are explicitly treated by the model (Section 2.2 and Table B.1). Table 3 summarizes mean values and standard deviations of maximum LUE measurements reported in the literature for different vegetation types, converted into units of mol CO_2 (mol APAR)$^{-1}$ as described by Anderson et al. (2000). These LUE values are based on annual or seasonal biomass accumulation from sites during time periods where climatic factors did not constrain photosynthesis (e.g., irrigated, highly productive sites), and represent here the aboveground and belowground net primary productivity (i.e., CO_2 uptake less autotrophic respiration) per mole PAR photons absorbed by the vegetation. The values have been standardized as suggested by Gower et al. (1999). As it was difficult to find literature values of β_n for C_4 grassland, this vegetation type was assigned a value of 0.03 according to Anderson et al. (2008).

Nominal C_i/C_a (γ_n) fractions have been determined through numerical experimentation with the Cupid model (Anderson et al., 2000) and reflect the distinctly different ratio of intercellular to ambient CO_2 concentration characteristic of canopies with C_3 and C_4 photosynthetic physiology (Wong et al., 1979; Baldocchi, 1994).

4.3. Scaled-leaf canopy sub-model

In comparison with the LUE module, the scaled-leaf module requires specification of significantly more adjustable parameters. The maximum catalytic capacity of Rubisco (V_m^{25}) and the potential rate of electron transport (J_m^{25}) at a temperature of 25 °C are critical species-specific parameters as species differ to a considerable extent in their biochemical capacity to assimilate CO_2 (Wullschleger, 1993). Vegetation-specific data on V_m^{25} for C_3 vegetation were derived based on estimates compiled by Wullschleger (1993) for 109 species representing several broad plant categories and by Kattge and Knorr (2007) for 36 species covering broadleaved trees and shrubs, coniferous tree needles and grasses, and Dreyer et al. (2001) provided estimates for temperature deciduous trees. The average and standard deviation of the compiled data for vegetation groups of relevance in this study are listed in Table 4. Very little information is available in the literature on the value of V_m^{25} for C_4 grasses and C_4 crops. For corn, a value of 30 μmol m^{-2} s^{-1} was used in accordance with leaf gas exchange measurements in maize reported in Massad et al. (2007) and Crafts-Brandner and Salvucci (2002). C_4 grasses were assigned a value of 20 μmol m^{-2} s^{-1} following Chen et al. (1994) and Kubien and Sage (2004). The electron transport rate (J_m^{25}), leaf respiration (R_d) and the initial slope of photosynthetic CO_2 response (k) were all parameterized as a function of V_m^{25} assuming that they co-vary with leaf nitrogen (e.g., Collatz et al., 1991; Collatz et al., 1992; Wullschleger, 1993). The relationship between V_m^{25} and J_m^{25} has been widely investigated and these two component processes have been shown to be tightly coupled with reported J_m^{25}/V_m^{25} ratios of e.g., 1.67 (Medlyn et al., 2002), 1.89 (Kattge and Knorr, 2007), 2.0 (Leuning, 2002) and 2.1 (Wohlfahrt et al., 1999). An arithmetic mean of these estimates was used here for all vegetation classes since the cause of the variation (e.g., species-specific differences, environmental conditions) is currently not clear. The R_d was assumed to equal 0.015 times V_m^{25} for C_3 plants and 0.025 times V_m^{25} for C_4 plants (Sellers et al., 1996). The nitrogen extinction coefficient (K_n) was fixed to 0.5 for the forest classes (Kellomaki and Wang, 2000) and to 0.7 for the remaining vegetation classes (De Pury and Farquhar, 1997) to

Table 3
Mean and standard deviations (stdd) among measurements of maximum LUE for major vegetation groups. All LUE values have been converted to units of mol CO_2 mol^{-1} from their original units of g NPP per MJ APAR as described in Anderson et al. (2000). N indicates the number of LUE estimates used to compute the average and standard deviation.

Vegetation type	N	Average LUE	Stdd in LUE	References
C_3 cropland (soybean)	3	0.024	0.001	Gower et al. (1999)
C_4 cropland (corn)	6	0.040	0.002	Gower et al. (1999)
Temperate evergreen needle-leaf	18	0.014	0.003	Gower et al. (1999), Ruimy et al. (1994), Runyon et al. (1994)
Temperate deciduous	8	0.020	0.006	Gower et al. (1999), Ruimy et al. (1994)
Temperate grasses	3	0.013	0.003	Ruimy et al. (1994), Kim and Verma (1990)
C_4 grasses	1	0.030	–	Anderson et al. (2008)
Desert shrubs	1	0.020	–	Gutschick (1996)

Table 4
Vegetation-specific V_m^{25} data based on estimates compiled in various studies. N indicates the number of V_m^{25} estimates used to compute the average and standard deviation (stdd). Values by Wullschleger (1993) are based on leaf temperatures corrected to a common reference temperature of 25 °C using a peaked Arrhenius temperature response function (Eq. (A.14)).

Vegetation classes	N	Average V_m^{25}	Stdd in V_m^{25}	Reference
C_3 cropland (soybean)	7	95	38	Wullschleger (1993), Kattge and Knorr (2007)
C_4 cropland (corn)	2	30	–	Massad et al. (2007), Crafts-Brandner and Salvucci (2002)
Temperate evergreen needle-leaf	18	49	30	Wullschleger (1993), Kattge and Knorr (2007)
Temperate deciduous	34	54	28	Wullschleger (1993), Kattge and Knorr (2007),Dreyer et al. (2001)
Temperate grasses	12	63	14	Wullschleger (1993), Kattge and Knorr (2007)
C_4 grasses	2	20	–	Chen et al. (1994), Kubien and Sage (2004)
Desert shrubs	3	122	28	Wullschleger (1993), Kattge and Knorr (2007)

simulate a slower decreasing rate of nitrogen concentration within forest canopies.

Ehleringer and Pearcy (1983) found the quantum yield for CO_2 uptake, α', to be similar for a wide range of monocot and dicot C_3 species with a representative average value of approximately 0.06 at a reference temperature of 25 °C. The α' parameter was converted into the quantum yield of electron transport (α_3) following von Caemmerer von and Farquhar (1981), using $\alpha = 4\alpha'(C_i + 2\Gamma^*)/(C_i - \Gamma^*)$ and fixing C_i to 280 μmol mol^{-1}. The resultant quantum yield ($\alpha_3 = 0.367$) was adopted for all simulations (Table 2). Ehleringer and Pearcy (1983) reported a larger systematic variability in the quantum yield for CO_2 uptake among C_4 species (α_4), and in accordance with their findings α_4 was set to 0.067 and 0.062 mol mol^{-1} for C_4 grasses and maize, respectively. The value of the curvature parameter, θ_j, that acts to smooth the transition between J_m and APAR (Eq. (A.4)) has been taken to be 0.7 (De Pury and Farquhar, 1997). The fitted values for the parameters θ_3, θ_4, β_3, and β_4, which control the degree of co-limitation between C_3 and C_4 photosynthetic rate limitations (Eq. (A.6)), are from Collatz et al. (1991, 1992).

The Michaelis–Menten coefficients of Rubisco activity for CO_2 (K_c^{25}) and O_2 (K_O^{25}), respectively, and the CO_2 compensation point in the absence of dark respiration (Γ^{*25}) are thought to be intrinsic properties of the Rubisco enzyme (Caemmerer von et al., 1994). Still, values reported in the literature at a reference temperature of 25 °C vary considerably. The values used here were determined from leaf gas exchange measurements on tobacco leaves (Bernacchi et al., 2001) and are similar to values reported by Farquhar et al. (1980). The photosynthetic rate constants defined at a reference temperature of 25 °C (V_m^{25}, J_m^{25}) were adjusted for different leaf temperatures using energies of activation (E_a) and deactivation (H_d) derived as the average of gas exchange data compiled from 36 plant species (Kattge and Knorr, 2007). Activation energies for K_c^{25}, K_O^{25} and Γ^{*25} were adopted from Bernacchi et al. (2001).

4.4. Seasonal variations in photosynthetic efficiency

Considering temporal or physiological changes in V_m^{25} has been shown to be important for determining the seasonality and magnitude of the net CO_2 assimilation rate for deciduous broadleaf trees (Wilson et al., 2001; Kosugi et al., 2003; Xu and Baldocchi, 2003). These studies generally reported (1) a rapid increase in V_m^{25} during leaf expansion and development, (2) maximum values of V_m^{25} during the early stages of leaf maturity, and (3) a fairly rapid decrease in V_m^{25} during leaf senescence irrespective of species type. Flux tower studies also suggest that LUE changes with time in the growing season for deciduous forest and agricultural sites and the decline in LUE towards the end of the growing season is associated with a decrease in foliar nitrogen concentration (Turner et al., 2003). Leaf nitrogen and chlorophyll content are significantly correlated with LUE (Gitelson et al., 2006) and V_m^{25} (Nijs et al., 1995) and recently Houborg et al. (2009) reported seasonal trends in leaf chlorophyll for a corn field similar to trends in the photosynthetic capacity of temperate deciduous forests observed by Wilson et al. (2000) and Kosugi et al. (2003). To test the improvement in model predictions by incorporating temporal changes, both models were run with fixed V_m^{25} and β_n, and with values that varied seasonally for the agricultural and deciduous forest sites. The scheme adopted here assumes that V_m^{25} and β_n scale linearly with green leaf area index ($L \times f_g$) from a minimum ($V_{m,min}{}^{25}$, $\beta_{n,min}$) during leaf emergence or complete senescence to a maximum ($V_{m,max}{}^{25}$, $\beta_{n,max}$) at peak green leaf area index (L_{max})

$$V_m^{25}(t) = V_{m,min}^{25} + \frac{L \times f_g}{L_{max}}(V_{m,max}^{25} - V_{m,min}^{25}) \quad (1)$$

$$\beta_n(t) = \beta_{n,min} + \frac{L \times f_g}{L_{max}}(\beta_{n,max} - \beta_{n,min}) \quad (2)$$

Seasonal trends in photosynthetic efficiency were not incorporated for the grassland sites as the succession of plant development stages typically observed in forests and croplands (i.e., leaf green up, maturity, senescence) may not be observed in grasslands due to e.g., grazing and multiple harvests for forage.

4.5. Respiration corrections

The CO_2 fluxes measured at the flux tower sites may include respiratory contributions from leaves (R_d), stems/bole (R_b) and soil/roots (R_s). The R_d and R_b are implicitly factored into the net CO_2 uptakes calculated by the LUE-based canopy sub-model as the nominal LUE values reported in Table 2 were based on estimates of above-ground and below-ground net primary productivity. In the scaled-leaf sub-model, leaf growth and maintenance respiration are accounted for by the temperature dependent dark respiration rate (Eq. (A.13)) but there is no correction for bole respiration, which can be an important component of total autotrophic respiration in forests (Amthor, 1989). Bole respiration at the two forest sites (BH and WB) was computed using the equation (e.g., Edwards and Hanson, 1996):

$$R_b = R_b^{10} Q_{10}^{(T_b - 10)/10} \quad (3)$$

where R_b^{10} is the bole respiration rate at 10 °C, Q_{10} is the relative increase in respiration rate for a 10 °C increase in temperature, and T_b is the bole temperature. The R_b^{10} at WB was fixed to 0.43 μmol m^{-2} s^{-1} according to Baldocchi (1997) and Edwards and Hanson (1996) and this value was also assumed to be representative for the ponderosa pine site (BH) (Ryan et al., 1995). The temperature sensitivity of R_b was modeled using a Q_{10} value of 2 (Amthor, 1989) and T_b was approximated as the average of the soil temperature at 10-cm soil depth and air temperature at the reference height above the canopy.

The total bulk ecosystem respiration originates from both below-ground autotrophic (i.e., roots) and heterotrophic (i.e.,

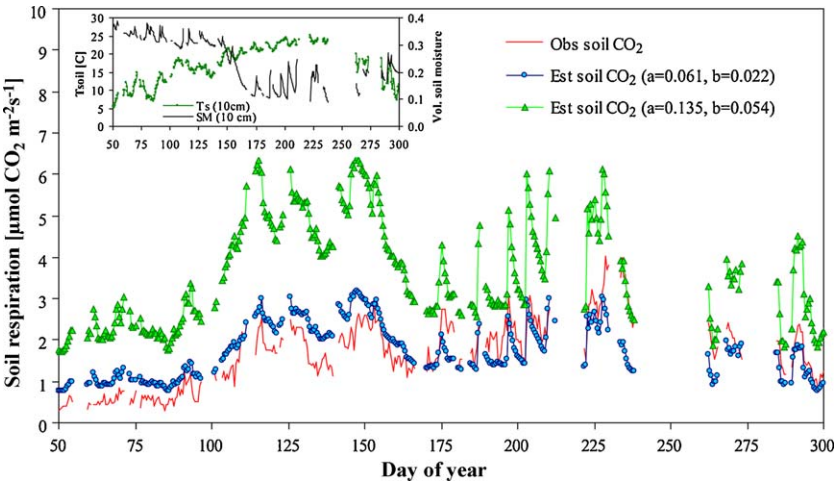

Fig. 2. Comparison of predicted and measured soil surface CO_2 fluxes at the Chesnut Ridge deciduous forest site for the year 2006. Estimates were based on the empirical soil respiration model developed by Norman et al. (1992) that takes into consideration the effect of root density, soil temperature and soil humidity (see inset). Soil respiration estimates based on original (triangles) and re-fitted (circles) regression constants are depicted.

microbial) respiration. In order to compare the estimated canopy CO_2 uptakes with the flux measurements, this soil respiration component (upward flux positive by convention) must be added to the net ecosystem exchange rate measurements. The empirical soil respiration model developed by Norman et al. (1992) for a tall-grass prairie in Kansas has demonstrated its effectiveness in reproducing observed soil respiration fluxes in other grassland, prairie and agricultural ecosystems (Wagai et al., 1998; Anderson et al., 2008) with root-mean-square deviations on the order of 1 μmol m^{-2} s^{-1}. The model includes the effect of soil temperature ($T_{s,10}$) and volumetric soil moisture content (W_{10}) near the surface (10 cm) and the density of roots in the form of a surrogate variable, the leaf area index (L), as described by

$$R_s = (a + b \times L)W_{10}\exp(0.069(T_{s,10} - 25)) \quad (4)$$

where a and b are site-specific regression constants given as 0.135 and 0.054, respectively for the tall-grass prairie site in Kansas (Norman et al., 1992). The applicability of Eq. (4) for reproducing forest floor CO_2 respiration fluxes was tested using hourly chamber measurements at the base of the Chestnut Ridge flux tower located in the same deciduous forest as the Walker Branch flux tower about 5 km to the northeast. Fig. 2 shows a comparison of predicted and measured soil surface CO_2 fluxes averaged over 12 h intervals (6 a.m.–6 p.m. and 6 p.m.–6 a.m.). Using the original regression constants results in large flux discrepancies particularly during the green up period (DOY 100–150) and later in the season when abrupt drops in soil moisture contents (see inset in Fig. 2) are coincident with peak vegetation densities. Re-fitting the soil respiration model using the 2006 data yielded values of 0.061 and 0.022 for the a and b regression coefficients, respectively, which corresponds to a ~55% reduction of the original parameter values. The re-calibrated model generally captures fluctuations caused by variations in soil temperature and soil moisture (see inset in Fig. 2) with a root-mean-square difference (RMSD) of only 0.53 μmol m^{-2} s^{-1} for the year 2006, the result of placing lower weights on L and W_{10} in Eq. (4). Model predictions using the re-fitted regression constants compared well with observations made during 2007 (RMSD = 0.85 μmol m^{-2} s^{-1}). The re-fitted model was also applied to the BH dataset assuming similarity in the magnitudes of soil respiration at some reference soil temperature and soil moisture content for these two forest ecosystems, while Eq. (4) with the original coefficients was used for the grassland and agricultural sites.

5. Model validation and intercomparisons

5.1. Carbon and latent heat fluxes

The LUE-based and scaled-leaf versions of ALEX were run at each of the seven flux tower sites (Table 1) using meteorological forcing data acquired at half-hourly intervals and seasonally fixed values of β_n and V_m^{25} (i.e., seasonal corrections described in Eqs. (1) and (2) were not applied). The overall agreement between ALEX simulations and eddy-covariance measurements of net carbon assimilation and evapotranspiration fluxes is quantified in Tables 5a and 5b. The model performances are assessed using the root-mean-square difference (RMSD), mean-bias-error (MBE), mean-absolute-error (MAE), and coefficient of determination (R^2) statistical descriptors and represent the average performance over the entire period of flux simulations. To facilitate an effective intercomparison of the two photosynthesis canopy sub-models, the flux comparisons have been restricted to daytime hours on days with green vegetation present, applying a threshold of APAR > 10 μmol m^{-2} s^{-1}.

Both canopy sub-models do reasonably well at reproducing the observed magnitudes and variances of carbon and water vapor exchange on half-hourly (Table 5a) and daily timescales (Table 5b). Half-hourly carbon flux simulations by the LUE-based sub-model account for 82–84%, 41–68%, and 41–60% of the variance in measurements from agricultural, grassland, and forest sites, respectively (Table 5a). While carbon flux simulations by the scaled-leaf model are comparable in accuracy, the flux validation generally yielded slightly lower R^2 values and slightly higher RMSDs and MAEs. Both models tend to overestimate carbon fluxes at the soybean (MBE = 0.8–1.1 μmol m^{-2} s^{-1}), corn (MBE = 4.2–4.9 μmol m^{-2} s^{-1}) and deciduous forest sites (MBE = 0.2–3.0 μmol m^{-2} s^{-1}). The agreement (i.e. R^2) between model calculations and measurements improve markedly when comparing daily integrated carbon flux data (Table 5b). Kellomaki and Wang (2000) and Anderson et al. (2000) also saw an improvement in the coefficient of determination when averaging hourly flux data between sunrise and sunset. The correlation between measurements and estimates from both models remains poor for the ponderosa pine site in Black Hills. Law et al. (2000) and Anderson et al. (2000) also reported low R^2 values for evergreen needle-leaf forest.

For the purpose of model testing, it has been argued that eddy flux measurements of carbon and water should be averaged by

Table 5a
Quantitative measures of the overall performance of the LUE (lue) and scaled-leaf (mec) based versions of ALEX in estimating half-hourly integrated carbon and latent heat fluxes. The statistics are representative of daytime hours with vegetation on the ground (APAR > 10 μmol m^{-2} s^{-1}).

Flux	Vegetation	Half-hourly validation statistics									
		N	*O*	RMSD		MBE		MAE		R^2	
				lue	mec	lue	mec	lue	mec	lue	mec
A_c	Soybean (BV, BP)	6545	15.3	5.4	6.4	1.1	0.8	4.1	4.8	0.82	0.72
	Corn (BV, BP)	7161	19.1	8.5	9.3	4.2	4.9	6.9	7.1	0.84	0.82
	Grassland (AG)	18210	2.2	2.4	2.7	0.8	0.8	1.8	1.8	0.63	0.68
	Grassland (FP)	10355	5.1	2.9	3.0	0.4	0.3	2.2	2.3	0.41	0.44
	Grassland (GC)	12640	13.1	4.0	4.7	−1.1	−0.5	3.1	3.6	0.68	0.56
	Conifer (BH)	10295	5.8	3.3	3.6	0.4	0.4	2.4	2.8	0.41	0.31
	Deciduous (WB)	7622	14.7	9.0	8.9	3.0	0.2	7.1	7.0	0.60	0.45
LE	Soybean (BV, BP)	7591	183	59	56	10	7	44	41	0.85	0.87
	Corn (BV,BP)	7980	174	56	56	−3	7	42	42	0.86	0.86
	Grassland (AG)	20776	62	34	41	6	16	24	31	0.77	0.72
	Grassland (FP)	12451	91	50	48	15	13	35	36	0.72	0.71
	Grassland (GC)	13651	167	45	53	8	−5	32	36	0.87	0.82
	Conifer (BH)	10630	111	58	60	−20	−12	42	45	0.65	0.59
	Deciduous (WB)	8037	181	80	83	36	23	60	63	0.79	0.73

N is the number of observations, *O* is the mean of the observations, RMSD is the root-mean-square difference between model estimates and measurements, MBE is the mean bias error (if negative the model underestimates measurements), MAE is the mean absolute error, and R^2 is the coefficient of determination. *O*, RMSD, MBE, and MAE have units of μmol m^{-2} s^{-1} (A_c) and W m^{-2} (LE).

Table 5b
As in (a) but for daily integrated fluxes. O, RMSD, MBE, and MAE have units of g C m^{-2} day^{-1} (A_c) and MJ m^{-2} day^{-1} (LE).

Flux	Vegetation	Daily integrated validation statistics									
		N	*O*	RMSD		MBE		MAE		R^2	
				lue	mec	lue	mec	lue	mec	lue	mec
A_c	Soybean (BV, BP)	251	31.3	6.5	7.6	2.3	1.6	5.4	6.3	0.89	0.82
	Corn (BV, BP)	274	37.0	12.5	14.2	8.8	10.2	10.5	11.7	0.89	0.85
	Grassland (AG)	785	3.8	3.4	3.7	1.3	1.4	2.7	2.7	0.80	0.82
	Grassland (FP)	367	11.3	3.8	4.6	0.7	0.7	3.2	3.9	0.66	0.61
	Grassland (GC)	530	24.7	5.6	5.6	−2.1	−1.0	4.7	4.5	0.68	0.67
	Conifer (BH)	388	12.3	4.0	4.4	0.7	0.7	3.0	3.4	0.39	0.33
	Deciduous (WB)	309	28.0	10.2	9.4	3.3	0.9	9.0	8.4	0.78	0.81
LE	Soybean (BV, BP)	288	8.5	1.8	1.4	0.5	0.3	1.4	1.1	0.81	0.89
	Corn (BV, BP)	304	7.8	1.6	1.7	−0.1	0.4	1.3	1.4	0.87	0.85
	Grassland (AG)	897	2.5	0.8	1.1	0.2	0.7	0.6	0.9	0.89	0.82
	Grassland (FP)	446	5.6	1.7	1.7	0.8	0.7	1.4	1.3	0.77	0.81
	Grassland (GC)	550	7.4	1.3	1.4	0.3	−0.3	1.0	1.1	0.83	0.80
	Conifer (BH)	404	5.2	1.7	1.6	−1.0	−0.6	1.3	1.2	0.69	0.66
	Deciduous (WB)	321	8.0	2.2	2.1	1.2	0.9	1.7	1.7	0.78	0.80

time to reduce random errors in the measurements and the natural variability that is associated with individual periods (Moncrieff et al., 1996; Baldocchi and Wilson, 2001). Sorting the fluxes by hour and averaging over 10-day periods improve the R^2 statistics of the carbon and latent heat flux simulations for most sites (Table 6). While the carbon flux R^2 remains low for the grassland (FP) and deciduous forest site, the MAEs are reduced significantly for all sites (Table 6). Noteworthy is the improved performance of the latent heat flux simulations (Table 6) where coefficient of determinations and MAEs now range from respectively, 0.80 to 0.93 and 16 to 47 W m^{-2} compared to 0.65–0.86 and 24–60 W m^{-2} before (LUE-based simulations). Overall the LUE-based model simulations are seen to account for more of the variance in the measurements than the scaled-leaf model simulations.

5.2. Temporal variations in carbon fluxes

The statistics reported in Tables 5a, 5b and 6 do not address seasonal and interannual variations in the agreement between model simulations and eddy-covariance measurements. Fig. 3 demonstrates the ability of the two models to reproduce temporal

Table 6
Coefficient of determinations (R^2) and mean-absolute-error (MAE) of the LUE (lue) and scaled-leaf (mec) based versions of ALEX in estimating hourly carbon and latent heat fluxes when the flux data have been sorted by hour and averaged for 10-day periods. The statistics are representative of daytime hours with vegetation on the ground (APAR > 10 μmol m^{-2} s^{-1}).

Flux	Vegetation	R^2		MAE	
		lue	mec	lue	mec
A_c	Soybean	0.90	0.87	2.8	3.2
	Corn	0.89	0.88	5.2	5.1
	Grassland (AG)	0.73	0.71	1.6	1.6
	Grassland (FP)	0.56	0.55	1.8	2.0
	Grassland (GC)	0.81	0.75	2.6	2.8
	Conifer	0.70	0.49	1.5	1.9
	Deciduous forest	0.54	0.44	5.3	5.7
LE	Soybean	0.88	0.91	34	30
	Corn	0.93	0.93	29	29
	Grassland (AG)	0.90	0.85	16	23
	Grassland (FP)	0.80	0.78	27	28
	Grassland (GC)	0.91	0.89	23	27
	Conifer	0.80	0.75	30	33
	Deciduous forest	0.86	0.82	47	47

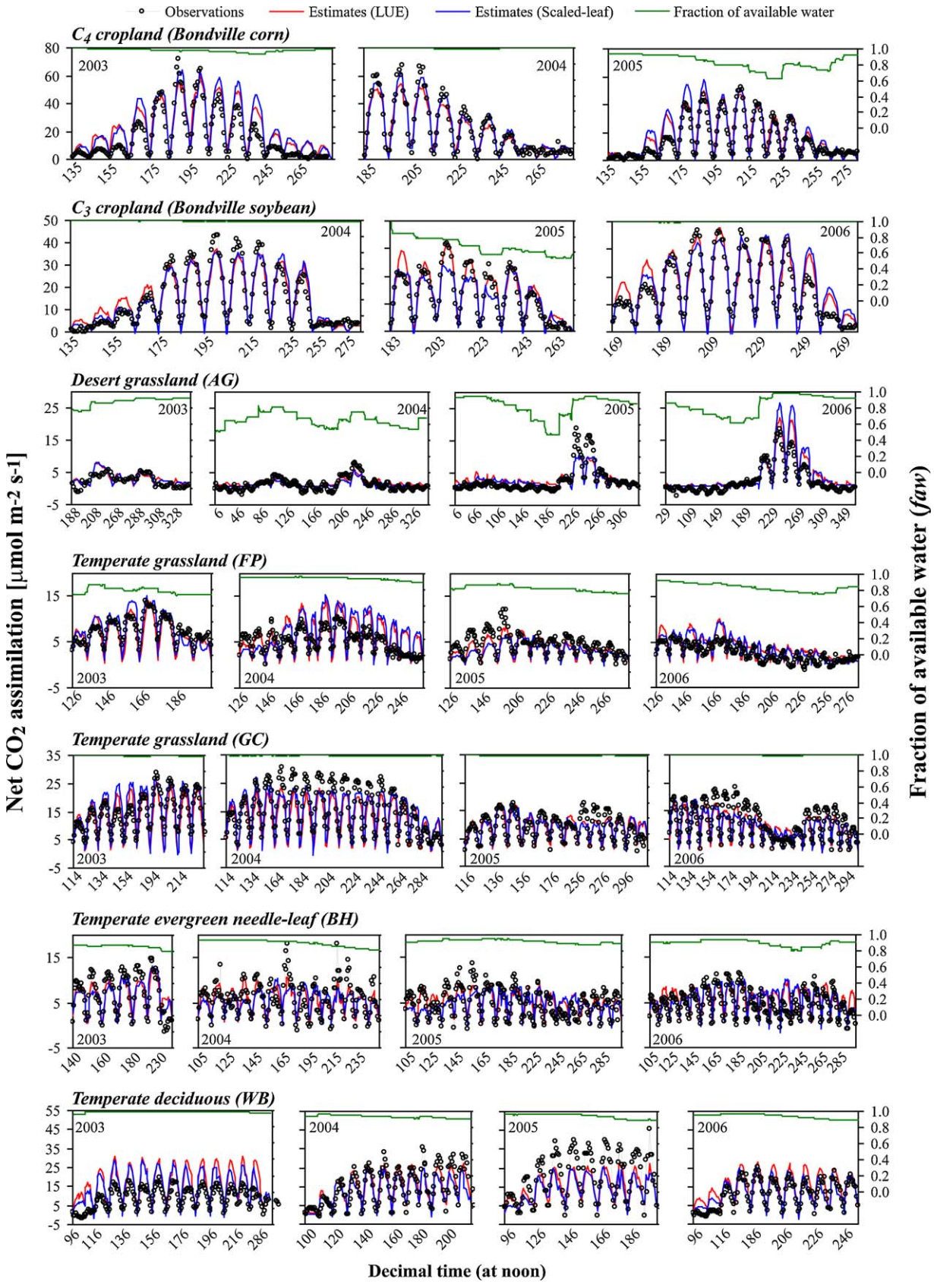

Fig. 3. The ability of the scaled-leaf and LUE-based models to reproduce temporal (diurnal, seasonal and interannual) patterns and magnitudes of CO_2 exchange over periods of 3–4 years at each flux tower site. For illustrative purposes, each diurnal segment represents flux data averaged by hour (daytime only) over 10-day intervals.

(diurnal, seasonal and interannual) patterns and magnitudes of net CO_2 assimilation (A_c) over periods of 3–4 years at each flux tower site. For illustrative purposes, each diurnal segment represents flux data averaged by hour (daytime only) over 10-day intervals, as in Table 6. Since the data have not been gap-filled, the flux records are not complete for all years. The time evolution of the modeled fraction of available water (*faw*) is also plotted to illustrate periods with soil–water-limited CO_2 assimilation rates ($faw < 1$).

While both models are successful in reproducing A_c during the leaf maturity stage at the corn and soybean sites, the biases reported in Table 5 are the result of overestimations early in the season during leaf expansion (~DOY 130–180), toward the end of the leaf maturity stage and during leaf senescence (>DOY 220) (Fig. 3). A similar temporal behavior in model overestimation is observed at the deciduous forest site in 2006. These seasonal trends in A_c may be associated with seasonal dynamics in photosynthetic efficiency, which has been shown to vary over the course of a season as leaves expand, age and senesce (Wilson et al., 2000; Kosugi et al., 2003; Xu and Baldocchi, 2003). Early-season biases may also reflect seasonal variations in leaf respiration. As leaf respiration at 25 °C is modeled as a constant fraction of V_m^{25} and leaf respiratory components are implicitly incorporated in the estimates of β_n, when V_m^{25} and β_n are fixed, neither model is able to capture the observed tendency towards peak respiration rates during leaf development and gradually declining rates as leaves mature (Xu and Baldocchi, 2003; Wilson et al., 2001). Model runs with seasonally varying V_m^{25} and β_n are presented and discussed in Section 5.4.

Midday and early afternoon depressions in assimilation rates modeled by the scaled-leaf model are particularly pronounced during the 2005 dry spell (~DOY 205–225) at the soybean site. Air temperatures were typically around 30 °C and winds were generally very calm (< 2 m s^{-1}), resulting in modeled sunlit leaf temperatures on the order of 40–45 °C. At these high temperatures, the applied temperature response functions (Eq. (A.14)) cause deactivation of V_m and J_m at rates determined by their respective deactivation energies (H_d, Table 2). The kinetic rate constants adopted here implicitly assume an optimum temperature for photosynthesis (T_{opt}) of 32 °C and a gradual decrease in activity above this temperature (Kattge and Knorr, 2007). However, the fact that observed assimilation fluxes do not show significant midday depression during this period suggests that T_{opt} should be higher for soybean. In fact Kattge and Knorr (2007) and Medlyn et al. (2002) reported a T_{opt} of 41 °C for soybean cultivars. Fig. 4 demonstrates the effect of the deactivation term in the generalized temperature response function on A_c for selected flux records averaged by hour over 10-day periods. Significant deviations in flux estimates begin to occur at canopy temperatures (T_c) exceeding 25 °C as the peaked (deactivation) and regular

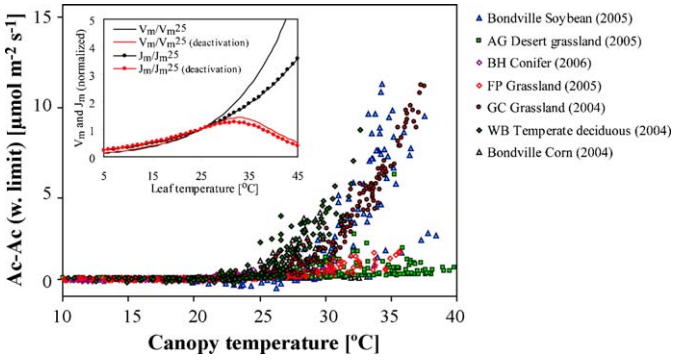

Fig. 4. The effect of a gradual deactivation of V_m and J_m on CO_2 assimilation (A_c) for selected flux records. The inset depicts normalized temperature response functions with and without the deactivation term.

(no deactivation) Arrhenius functions diverge (see inset in Fig. 4). Hourly carbon fluxes are seen to increase by up to ~12 μmol m^{-2} s^{-1} if the deactivation is neglected and V_m and J_m are allowed to keep increasing at the rate determined by their respective activation energies (Fig. 4). The gradual deactivation of photosynthesis at canopy temperatures above 32 °C likely initiates a feedback loop that may increase T_c to an unrealistic level; The initially reduced CO_2 assimilation rate causes a higher stomatal resistance leading to a decrease in the latent heat flux and a greater fraction of the available energy being partitioned into sensible heating, which will then increase T_c and thereby decreasing A_c even further. While the overall MAE of simulated CO_2 assimilation rates at the soybean and deciduous forest sites decrease slightly from 3.2 and 5.8 to 3.1 and 5.1 μmol m^{-2} s^{-1}, respectively, as a result of running ALEX without temperature deactivation, the corn and Goodwin Creek grassland sites see a significant increase in overall MAE from 5.1 and 2.8 to 6.6 and 4.8 μmol m^{-2} s^{-1}, respectively. Whether temperature limitations of V_m and J_m occur is a debatable issue. Kattge and Knorr (2007) demonstrated a tendency for an acclimation response of V_m and J_m to plant growth temperatures with optimum temperatures for 36 species ranging from 20 to 50 °C. Dreyer et al. (2001) reported the temperature optima of seven temperate tree species to range between 35.9 and above 45 °C whereas Bernacchi et al. (2001) found that the addition of a deactivation term was unnecessary at temperatures <40 °C. Based on the findings here, the use of species-specific temperature acclimation response functions may be critical for a successful implementation of the scaled-leaf model.

Fairly significant discrepancies between scaled-leaf and LUE-based model simulations occur early in the growing season at the temperate grassland site in Fort Peck, MT and the needle-leaf forest site in the Black Hills, SD (Fig. 3). At these northerly sites, daytime air temperatures below 10 °C are not unusual during the months of April and May (DOY 91–151). In the scaled-leaf model, low temperatures result in low photosynthetic capacities (Fig. 4 inset) which increase the likelihood of the CO_2 assimilation to become limited by the carbon compound export limited transport rate,(-$A_s = 0.5 \times V_m$; Eq. (A.5)). As a consequence, the scaled-leaf model typically underestimates the CO_2 flux at these sites early in the season (Fig. 3). This problem could be partially overcome by increasing the proportionality constant in Eq. (A.5), thereby weakening the influence of A_s. Other studies have indicated that the removal of assimilates (i.e. A_s) should not be the major limitation for plant growth (e.g., Soegaard and Nordstroem, 1999; Haxeltine and Prentice, 1996). In comparison, the LUE-based model estimates are generally in better agreement with the measurements. However, the LUE-based estimates are positively biased late in 2006 (DOY 290–300) at the needle-leaf forest site (Fig. 3). During this time period the average midday air temperature was 3.1 °C compared to 12.5 °C in the previous year and 6 days experienced air temperatures at or below 0 °C indicating that the effects of low temperatures on photosynthetic efficiency should not be neglected.

Both canopy models do a reasonable job at capturing seasonal and year-to-year variations in A_c at the three grassland sites (Fig. 3). At the desert grassland site, vegetation growth is impaired by soil water deficits ($faw < 1$) throughout much of the year but respond rapidly to rainfall events during the late summer monsoon season. The flux underestimation in 2005 and overestimation in 2006 during peak vegetative growth could be related to uncertainties in the estimation of a representative leaf area index (L). Tower-based observations of NDVI imply that L reached a maximum value of 1.1 and 3.1 in 2005 and 2006, respectively, although maximum observed assimilation fluxes were similar between the years. Field measurements of L for these years were

not available for the grassland and forest sites to verify the empirical NDVI relationships derived by Wilson and Meyers (2007). As the *NDVI* values are essentially point measurements, spatial heterogeneity in vegetation cover in the immediate vicinity of the Audubon flux tower could provide partial explanation for the large discrepancies between flux simulations and measurements for these years. Differences in flux footprint may also play a significant role at the evergreen needle-leaf forest site in the Black Hills as this site is quite heterogeneous and characterized by large open spaces (Wilson and Meyers, 2007).

Uncertainties related to the estimation of *faw* could be another significant source for biased flux simulations. While CO_2 fluxes at the Fort Peck grassland site are generally well-reproduced during 2003, 2005 and 2006 when ALEX simulates fairly significant soil water deficits (*faw* = 0.7–0.8), *faw* simulations during 2004 indicate ample soil moisture conditions (∼0.97) which causes the carbon fluxes to be overestimated by 31% on average. The site received a similar amount of precipitation (∼200 mm) during the May–September growing season in all 4 years. However, the initial soil moisture profile used as input to the soil transport module in 2004 was characterized by comparatively higher soil moisture contents due to a rainfall event just prior to the start of the simulations. The soil transport module modeled a too slow depletion of soil moisture from the root zone (not shown) which caused *faw* to remain high throughout much of the growing season. The estimation of *faw* depends heavily on the setting of the wilting point and field capacity soil moisture content, which are linked to soil type. In the current model setup the soil profile is assumed to have uniform hydraulic and thermal properties and this very simplistic treatment of soil processes can easily cause errors in the estimation of *faw* and thus canopy fluxes.

Carbon flux simulations at the deciduous forest site at Walker Branch diverge considerably from observations during 2003 and 2005 in particular (Fig. 3). Measured fluxes were almost 50% lower during the 2003 growing season despite it being the wettest season (∼830 mm compared to ∼650 during 2004–2006). Variations in the extent and composition of the upwind source area (i.e., footprint) of the fluxes measured at the tower could be one significant source of variance between measurements and model estimates as the composition of species (and possibly vegetation density) viewed by the tower is likely to change with wind direction and atmospheric stability in this mixed forest stand. In 2003 winds most frequently originated from south-southwesterly (S-SW) (34%) and southwest-westerly (SW-W) (19%) directions whereas winds from northeasterly to southeasterly (NE-E, E-SE, SE-S) directions were characterized by frequencies on the order of 8%. The wind regime was more variable in 2005 and winds originated from NE-E, E-SE, SE-S, S-SW and SW-W directions with very similar frequencies (∼15%). While forest species may differ to a considerable extent in their biochemical capacity to assimilate CO_2 from the atmosphere (Wullschleger, 1993), species-specific differences in photosynthetic efficiency have been shown to be not so important for determining the energy budget (Anderson et al., 2008) and the latent heat fluxes are reasonably reproduced in both years (Fig. 5). However an adjustment of β_n and V_m^{25} may be required to accommodate interannual variations in the species composition viewed by the flux tower and appears to be critical for modeling year-to-year carbon fluxes accurately at this site.

5.3. Temporal variations in latent heat fluxes

Fig. 5 and the associated statistics in Tables 5a, 5b and 6 demonstrate that both canopy sub-models reproduce temporal patterns and magnitudes of latent heat exchange with good fidelity. While both models use a similar formalism for calculating LE (Eqs. (A.11) and (B.1)), the value of the stomatal resistance will reflect differences in the photosynthesis models. Additionally, in the scaled-leaf model the derived LE is the sum of contributions from sunlit and shaded leaf fractions. Nevertheless, evaporative flux estimates from the two models tend to be highly intercorrelated. The largest LE divergences between the two models occur early in the season at the soybean, Fort Peck temperate grassland, and temperate deciduous forest sites and they generally correlate with the carbon flux divergences given joint dependence on the stomatal resistance. Despite difficulties in reproducing interannual variations in the carbon flux at the deciduous forest site in 2003 and 2005 (Fig. 3), latent heat flux is modeled more robustly. Reduced CO_2 assimilation rates as a result of deactivation of V_m and J_m (Section 5.2) will initially decrease LE due to a decrease in stomatal conductance. However the associated leaf temperature increase (Fig. 4) will increase the vapor pressure deficit thereby counterbalancing the stomatal conductance effect (Eq. (A.11)). The sensitivity analysis in Section 5.7 gives further indication that uncertainties related to A_c estimation generally have a reduced effect on LE.

The occasionally large discrepancies between estimated and measured flux quantities early in the seasons may be related to overestimates of the green leaf area index prior to leaf emergence (∼1.0, ∼0.5, and ∼0.2 at the temperate deciduous, soybean, and Fort Peck grassland sites, respectively) or possibly reflect uncertainties related to the estimation of soil evaporation in ALEX.

As previously mentioned, closure among energy flux components was enforced by modifying the observed sensible and latent heat fluxes such that they summed to the available $(R_n - G)$ energy yet retained the observed Bowen ratio (BR). On average, eddy-covariance latent heat fluxes were on the order of 10–25% lower than the BR-corrected fluxes at the cropland, evergreen needle-leaf and grassland sites except for Fort Peck where observed fluxes were 10% higher. At the deciduous forest site the latent heat fluxes measured by the eddy-covariance instrument underestimated the BR-corrected fluxes by 39% which suggests significant energy storage within the forest stand. Residually corrected latent heat fluxes (i.e., $LE = R_n - H - G$) were between 0% and 40% larger than the BR-corrected fluxes and resulted in degraded model performance at all sites (when compared to applying BR closure). The use of residually corrected fluxes in place of the uncorrected eddy-covariance measurements did however improve the fit with estimated fluxes at the Bondville, Fort Peck and Walker Branch sites.

5.4. Seasonality in photosynthetic efficiency

Carbon flux simulations based on the seasonal variation of V_m^{25} and β_n data are illustrated for soybean (C_3 cropland), corn (C_4 cropland), and deciduous forest sites in Fig. 6. The V_m^{25} and β_n were scaled linearly with green leaf area index using Eqs. (1) and (2), respectively. The $V_{m,min}^{25}$ and $\beta_{n,min}$ were parameterized as 15% (corn and forest) and 40% (soybean) of maximum V_m^{25} and β_n during green up, and set to zero during the late season decline corresponding to fully senescent leaf material (no photosynthetic activity). Maximum V_m^{25} and β_n correspond to the values listed in Table 2.

The fit between estimates and measurements is significantly improved at the cropland sites as a result of incorporating temporally varying V_m^{25} and β_n data (Fig. 6a and b). At the corn site, the MAE of the hourly 10-day averaged simulations during 2003 was reduced from 7.7 to 3.2 $\mu mol\ m^{-2}\ s^{-1}$ for the scaled-leaf model and from 7.4 to 3.7 $\mu mol\ m^{-2}\ s^{-1}$ for the LUE-based model. Similar model performance improvements were observed at the soybean site during 2006 where MAEs were reduced to 3.6 and 3.0 $\mu mol\ m^{-2}\ s^{-1}$ for the scaled-leaf and LUE-based models, respectively. Significant model performance improvements were also observed for the latent heat fluxes (not shown).

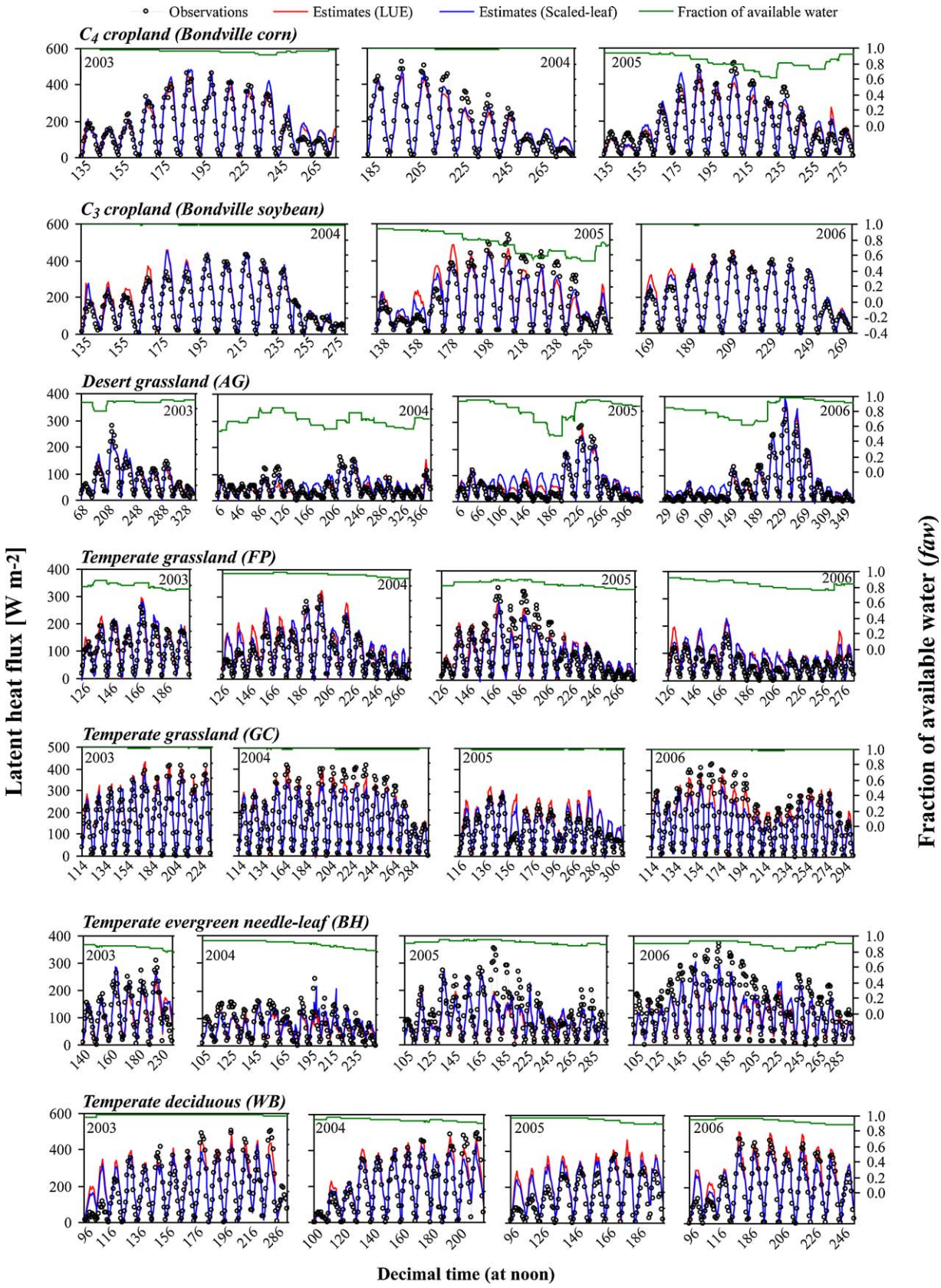

Fig. 5. The ability of the scaled-leaf and LUE-based models to reproduce temporal (diurnal, seasonal and interannual) patterns and magnitudes of latent heat exchange over periods of 3–4 years at each flux tower site. For illustrative purposes, each diurnal segment represents flux data averaged by hour (daytime only) over 10-day intervals.

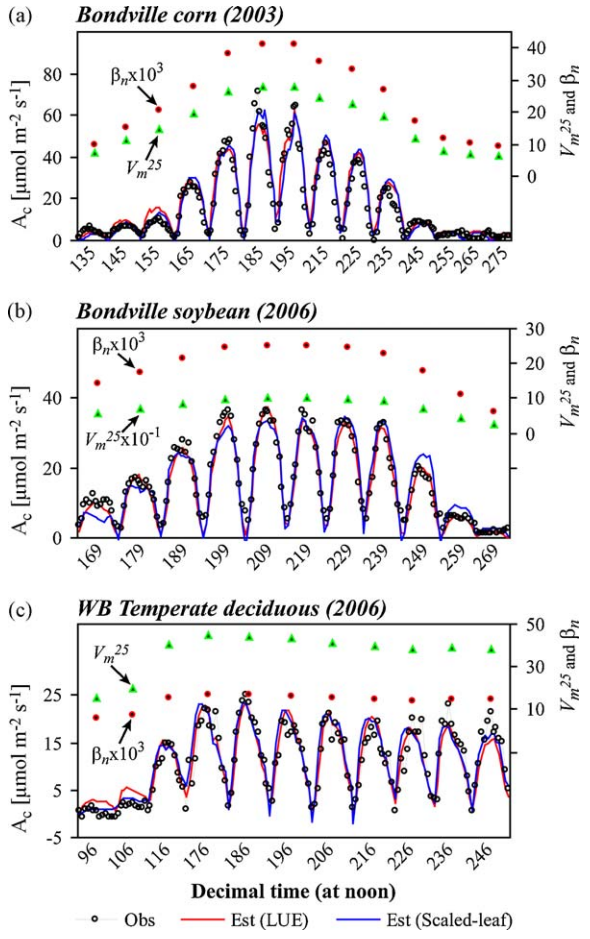

Fig. 6. Comparison between hourly carbon flux measurements and simulations based on seasonally changed V_m^{25} and β_n data for corn (a), soybean (b), and deciduous forest (c) sites. Note that each diurnal segment represents flux data averaged by hour (daytime only) over 10-day intervals.

At the forest site, the scaled-leaf model was run without the deactivation term in the temperature response functions for V_m and J_m. In this seasonal parameterization, the optimum phase of photosynthesis occurs in June and V_m and β_n only diverge slightly from their optimal values during the remainder of the depicted flux record due to moderate variations in L during this stage of leaf maturity (Fig. 6c). The flux record at the forest site is too short to capture the more rapid decline in photosynthetic capacity during the period of autumnal senescence reported in a number of studies (Xu and Baldocchi, 2003; Wilson et al., 2001; Kosugi et al., 2003). Wilson et al. (2001) reported more dynamics in V_m over the growing season in a deciduous forest stand and included leaf age specifically as a reducing factor after the spring maximum in V_m.

Evidently, some consideration of temporal changes in V_m and β_n is needed to reproduce the carbon fluxes with high fidelity at these sites. The simplified seasonal parameterization procedure demonstrated here causes variations in V_m and β_n during leaf development and senescence when changes in photosynthetic efficiency are most likely to occur, and is well suited to application over large regions as green leaf area index can be derived with reasonable accuracy from remote sensing.

5.5. Impact of light environment

CO_2 assimilation efficiency is known to increase with diffuse radiation conditions (e.g., Gu et al., 2002) as diffuse radiation is uniformly distributed over leaves in a canopy causing a small fraction of the leaves to experience light saturation. This phenomenon is treated very differently by the two canopy models. The scaled-leaf model responds to an increase in the fraction of PAR that is diffuse (f_{dif}) by partitioning a greater fraction of the PAR to the shaded fraction of leaves in the canopy. Shaded leaves typically operate in Rubisco limited mode (i.e., not limited by light) and therefore have larger light-use efficiencies. In the LUE-based model, the response to f_{dif} is based on simulations by the Cupid model (Norman and Arkebauer, 1991) that indicated a nearly linear response of LUE to f_{dif} (Eq. (B.8)). Fig. 7 illustrates the correspondence between hourly carbon flux simulations and measurements averaged over the growing seasons and sorted in intervals representing the fraction of diffuse radiation. Each segment represents the averaged hourly flux response during conditions throughout the growing seasons where the hourly fraction of diffuse radiation was within the specified interval (e.g., 0–0.1, 0.1–0.2). In most of the case studies, the scaled-leaf model reproduces A_c well during variable diffuse lighting conditions. The model underestimates fluxes at the grassland site around noon when the radiation above the canopy was mainly direct, which likely reflect high temperature deactivation of V_m and J_m (Section 5.2) as high temperature inhibition of photosynthesis is most likely to occur when the fraction of PAR absorbed by sunlit leaves is greatest. The fraction of PAR absorbed by the shaded fraction of the canopy increased from ~0.05 to ~0.6 when the light environment changed from mainly direct (f_{dif} = 0.05) to mainly diffuse (f_{dif} = 0.95).

The applied modification of β_n in the LUE model by changes in diffuse lighting is seen to be critical for matching flux simulations with measurements during conditions when more than 50% of the radiation is diffuse at the soybean (Fig. 7b), forest (Fig. 7c) and grassland (Fig. 7d) sites. The modification of β_n results in increases of up to 5 μmol m^{-2} s^{-1} in hourly averaged fluxes during mainly diffuse radiation conditions and decreases of up to 8 μmol m^{-2} s^{-1} during mainly direct radiation conditions (Fig. 7). The correction improves the agreement with observations over the full range in diffuse light as evidenced by reductions in half-hourly MAEs from 5.4, 3.8, 7.9 and 2.8 μmol m^{-2} s^{-1} to 5.2, 3.0, 6.6 and 2.5 μmol m^{-2} s^{-1} for the depicted corn, soybean, forest and grassland flux records, respectively. The minor effect of the β_n modification at the corn site (Fig. 7a) reflects the fact that leaves of C_4 species saturate at higher light levels than leaves of C_3 species and this tendency is supported by the model results. The LUE-based model tends to perform slightly better than the scaled-leaf model during predominantly direct radiation conditions but still underestimates measurements at the deciduous forest site. ALEX uses a fairly simplistic analytical formulation to describe light interception by canopies (Goudriaan, 1977; Anderson et al., 2000) that does not specifically treat the complexity of light penetration in forest stands (e.g., penumbral effects), and may result in underestimation of absorbed PAR and the fraction of absorbed PAR distributed on shaded leaves when radiation is primarily direct.

5.6. Intercomparisons of CO_2 concentration and light-use efficiency

Time-series of simulated ratios of intercellular to ambient CO_2 concentration (C_i/C_a) around noon are shown in Fig. 8a and b for the corn and soybean sites. The C_i/C_a ratio (γ) simulated by the LUE-based model fluctuates around the nominal value of C_i/C_a (γ_n) in response to changes in diffuse radiation conditions, stomatal conductance and soil water deficits. The LUE-based modeling paradigm assumes that the functional dependence of A_c on C_i becomes linearized on the canopy level (Anderson et al., 2000) and the derived γ values generally track the dynamics in γ simulated by the scaled-leaf model closely. The derived γ values are within the range you would normally expect for plants with C_4 and C_3

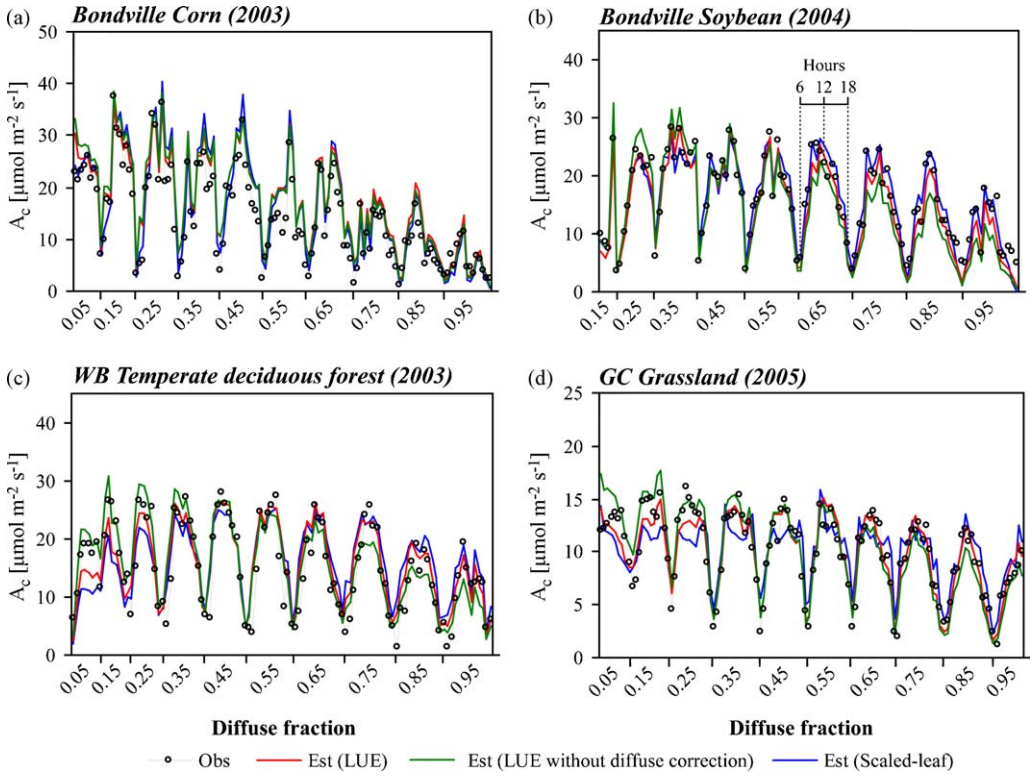

Fig. 7. The correspondence between hourly carbon flux simulations and measurements when sorted as a function of the fraction of diffuse radiation. Each diurnal segment (see (b)) represents the averaged hourly flux response during conditions throughout the growing season of each year where the diffuse radiation was within the specified interval.

photosynthetic pathways (Wong et al., 1979). Changes in γ are directly reflected in the actual light-use efficiencies calculated as A_c/APAR (Fig. 8c and d). The magnitude of the change in actual LUE from the seasonally changed nominal value (β_n–the over-plotted black solid line) is on the order of ±0.007 for the corn site and ±0.009 for the soybean site. Evidently, LUE-based carbon models that do not take into consideration the C_i–LUE response may face serious issues in tracking day-to-day variations in CO_2 assimilation fluxes.

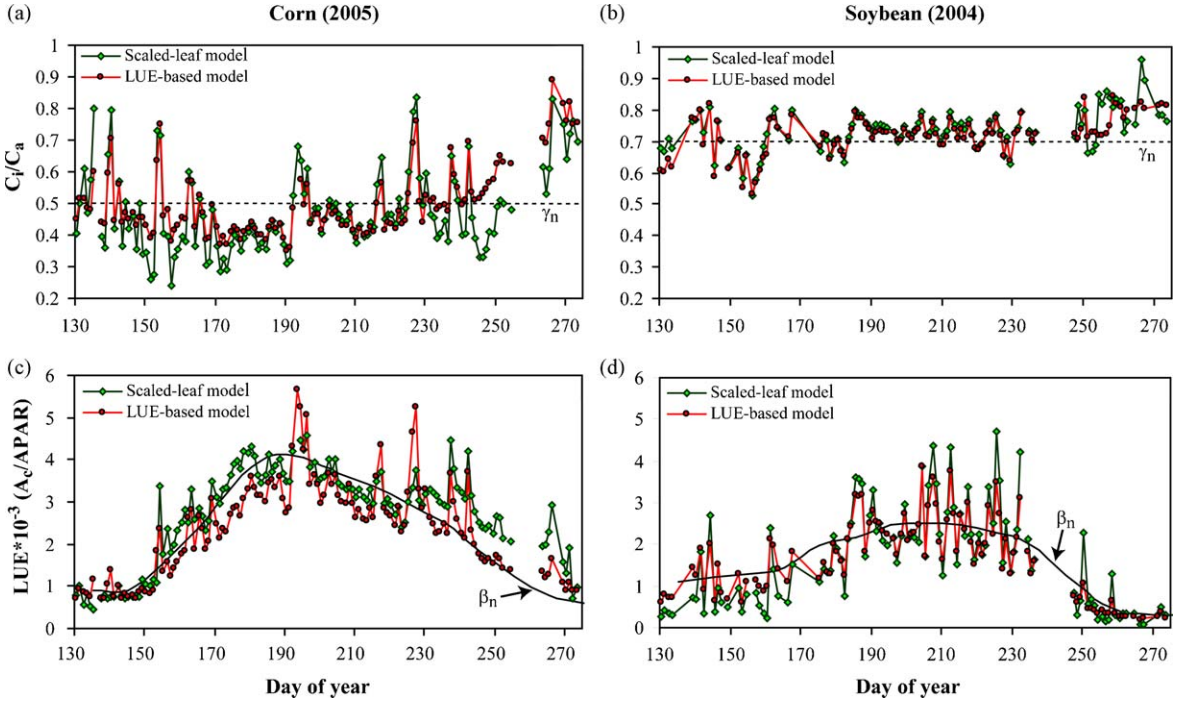

Fig. 8. Time-series of simulated ratios of intercellular to ambient CO_2 concentration (C_i/C_a) (a and b) and light-use efficiencies (LUE) (c and d) around noon for corn and soybean sites. Nominal values of C_i/C_a (γ_n) and LUE (β_n) are over-plotted with dotted and solid lines, respectively. Note that seasonally changed values of V_m^{25} and β_n (Section 5.4) have been used to generate these plots.

Table 7
Sensitivity of carbon and energy fluxes to variations in the adjustable parameters specific to each C_3 canopy sub-model, expressed as slopes of regressions lines. A slope greater than unity indicates that sensitivity run simulations overestimate reference run simulations. The sensitivity results were generated using the pattern of canopy development and environmental conditions observed during the 2004 growing season (May–September) at the Bondville (BV) soybean site.

C_3 cropland		Deviation in fluxes from reference			
Parameter	Sensitivity range (max, min)	A_c		LE	
		Max	Min	Max	Min
Scaled-leaf					
V_m^{25}	95 ± 40	1.17	0.75	1.05	0.91
J_m^{25}/V_m^{25}	1.9 ± 0.4	1.04	0.94	1.01	0.98
k_n	0.7 ± 0.3	0.98	1.02	0.99	1.01
α_3	0.37 ± 0.07	1.10	0.89	1.03	0.97
θ_j	0.7 ± 0.2	1.06	0.95	1.01	0.99
θ_3	0.9 ± 0.1	1.18	0.92	1.05	0.97
LUE-based					
β_n	0.024 ± 0.006	1.23	0.76	1.05	0.94
γ_n	0.7 ± 0.1	0.84	1.23	0.96	1.05

5.7. Sensitivity to variations in adjustable parameters

Discrepancies between model simulations and observations may be attributed to the values used for the adjustable canopy parameters specific to each canopy sub-model (Table 2). The sensitivity of the models to variations in key parameters was examined by linearly regressing nominal run model output with simulation results obtained using changed values of each sensitivity parameter at a time, while holding the others unchanged. The linear relationships were forced through zero intercept and the regression slopes were used to assess the average response of the applied changes in parameter values on the simulation results. Tables 7 and 8 present carbon and latent heat flux sensitivity results obtained when the adjustable parameters specific to each C_3 and C_4 canopy sub-model were changed as indicated. The half-hourly model simulations were based on model runs encompassing the entire growing season at the corn and soybean sites and thus represent a wide range of environmental and phenological conditions. The sensitivity of carbon flux simulations to variations in V_m^{25} is shown graphically in Fig. 9a and b for crops with C_3 and C_4 photosynthetic pathways, respectively. Increasing V_m^{25} from 95 to 135 μmol m^{-2} s^{-1} (C_3) and 30 to 40 μmol m^{-2} s^{-1} (C_4) lead to a 17% and 11% rise in A_c, respectively, while decreases of 25% and 17% are produced when V_m^{25} is reduced to 55 and 20 μmol m^{-2} s^{-1}, respectively. The latent heat flux (LE) is less sensitive to variations in photosynthetic capacity (Tables 7 and 8) as V_m^{25} acts indirectly on canopy transpiration through the stomatal conductance. Correspondingly, latent heat fluxes are seen to be significantly less sensitive to variations in the photosynthetic parameters J_m^{25}/V_m^{25}, k_n, α_3, θ_j, θ_3, k/V_m^{25}, α_4, θ_4, and β_4 than are CO_2 assimilation rates (Tables 7 and 8). The same tendency is evident in the sensitivity results for the LUE-based model (Tables 7 and 8), which supports other studies (e.g., Anderson et al., 2008; Leuning et al., 1998) that suggest that the choice of key photosynthesis model parameters is not so important for determining energy fluxes accurately.

The quantum yield for electron transport (α_3) and CO_2 uptake by C_4 plants (α_4) are critical parameters in the scaled-leaf model as A_c is seen to change with ~10% when α_3 and α_4 are varied as shown. Adopted values for α_3 typically vary between approximately 0.18 and 0.40 (Wullschleger, 1993; Harley et al., 1992; Medlyn et al., 2002; Leuning et al., 1998, Farquhar et al., 1980) and quantum yield may also exhibit seasonal patterns of variation (Gilmanov et al., 2005), which add to the uncertainty in their parameterization. Reported values of the J_m^{25}/V_m^{25} ratio vary widely from around 1.6 to ~3.3 (Medlyn et al., 2002; Kattge and Knorr, 2007; Leuning, 2002; Wohlfahrt et al., 1999) and J_m^{25}/V_m^{25} has also been show to vary over the growing season (Wilson et al., 2000). While variability in J_m^{25}/V_m^{25} has been related to differences in plant type and climate, results remain inconclusive and the use of a fixed ratio could lead to some model deficiencies for certain species or environments as modest variations in J_m^{25}/V_m^{25} ($\pm$ 0.4) change A_c by approximately 5% (Table 7). Increasing the C_3 and C_4 curvature (co-limitation) parameters (θ_3, θ_4) from 0.9 to 1.0 leads to an 18% and 12% increase in A_c, respectively, which makes the issue of the degree of co-limitation between electron transport (A_j) and Rubisco limited (A_v) CO_2 assimilation equally important to the parameterization of V_m^{25}. Interestingly, De Pury and Farquhar (1997) ignored the gradual

Table 8
As in Table 7 but using the pattern of canopy development and environmental conditions observed during the 2005 growing season (May–September) at the Bondville (BV) corn site.

C_4 cropland		Deviation in fluxes from reference			
Parameter	Sensitivity range (max,min)	A_c		LE	
		Max	Min	Max	Min
Scaled-leaf					
V_m^{25}	30 ± 10	1.11	0.83	1.03	0.95
k/V_m^{25}	$20 \times 10^3 \pm 10 \times 10^3$	1.01	0.98	1.00	0.99
k_n	0.7 ± 0.3	0.97	1.04	0.99	1.01
α_4	0.062 ± 0.01	1.08	0.90	1.02	0.97
θ_4	0.9 ± 0.1	1.12	0.94	1.03	0.98
β_4	0.9 ± 0.1	1.03	0.98	1.01	0.99
LUE-based					
β_n	0.042 ± 0.006	1.11	0.89	1.03	0.97
γ_n	0.5 ± 0.1	0.87	1.19	0.97	1.04

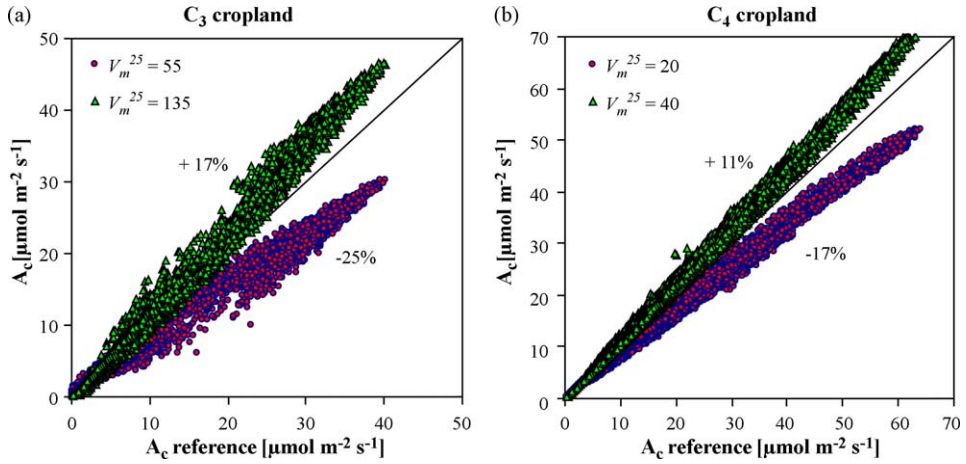

Fig. 9. The sensitivity of half-hourly carbon flux simulations by the scaled-leaf model to variations in V_m^{25} for crops with C_3 (a) and C_4 (b) photosynthetic pathways, respectively. The relative change in % in response to the applied changes is also shown.

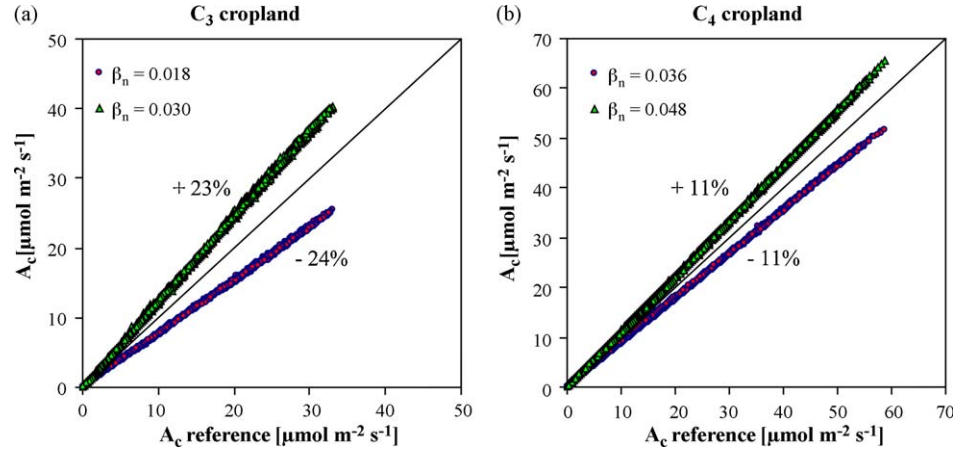

Fig. 10. The sensitivity of half-hourly carbon flux simulations by the LUE-based model to variations in nominal LUE (β_n) for crops with C_3 (a) and C_4 (b) photosynthetic pathways, respectively. The relative change in % in response to the applied changes is also shown.

transition between A_j and A_v completely arguing that co-limitation has little effect on C_3 canopy photosynthesis, as only a small fraction of leaves are near the transition to light saturation at any moment. In C_4 plants Collatz et al. (1992) observed a gradual saturation of A_c with respect to incident quantum flux which suggested significant co-limitation between A_j and A_v and a fitted curvature parameter significantly less than one.

In the LUE-based model parameterization, uncertainties are reduced to only two adjustable parameters that appear to be equally influential in modifying CO_2 assimilation rates (Fig. 10 and Tables 7 and 8). The response of A_c to the applied variations in nominal LUE (β_n) is approximately linear with characteristic changes of ±23% and ±11% for C_3 and C_4 plants, respectively while A_c is seen to be more sensitive to a decrease in nominal C_i/C_a (γ_n) than a corresponding increase in γ_n (Tables 7 and 8). While β_n (when representing nominal light-use-efficiency for unstressed vegetation) appears to be a fairly conservative quantity within major vegetation classes based on the compiled estimates listed in Table 3, the tabulated standard deviations were based on a fairly small number of samples. Additional intra-class variability in β_n may arise as a result of e.g., variability in respiratory behavior (i.e. respiration to assimilation ratio), stand age and vegetation nutrient status. Also, estimates of β_n are associated with several sources of uncertainty and inconsistencies as discussed in detail by Gower et al. (1999). However, approximating realistic β_n and γ_n values for major vegetation groups appears to be more straightforward than specifying the large number of leaf-scale parameters with acceptable accuracy for different species compositions and environments.

5.8. Model utility for larger-scale applications

As previously noted in Section 1, biophysical models intended for routine applications at larger scales should be capable of realistically simulating the response of CO_2 and energy fluxes to environmental and physiological forcings while remaining computationally inexpensive and sufficiently simple to be effectively parameterized. The two modeling paradigms presented in this study were both capable of reproducing observed magnitudes and patterns of carbon and water exchange for a wide range of environmental and phenological conditions with acceptable accuracy. While the system of equations for both models is solved using fast analytical solutions, the LUE-based version arrives at model solutions faster than the scaled-leaf version where a larger number of computations must be done for sunlit as well as shaded canopy fractions. The key difference between the two models is the model complexity (see Table A.1 and Table B.1) and the number of model parameters that must be specified, and the success of either paradigm relies on the validity of the chosen parameterizations. Section 4.3 demonstrated the considerable challenge involved in assigning representative values to the many species-dependent

parameters of the scaled-leaf model. These parameters represent conditions of individual leaves and are typically very difficult and time-consuming to measure routinely. The large variability associated with key parameters such as the maximum Rubisco capacity (Table 4) and the temperature response parameters (Section 5.2) adds to the uncertainty. The LUE-based model has the advantage of only requiring two parameters (Table 2) that have been found to be fairly conservative in nature within broad vegetation groups. As they represent canopy conditions they are more straightforward to evaluate for a diversity of agricultural and natural ecosystems either from biomass accumulation or directly from CO_2 eddy flux observations. Due to the embedded empiricism of this approach uncertainties associated with the mechanistic description of leaf-level processes and the leaf-to-canopy scaling assumptions are avoided. However as noted by Anderson et al. (2000) the embedded empirical relationships (Eqs. (B.7) and (B.8)) may need modification in response to a changing climate as they in principle only have usefulness within the range of conditions under which they were developed.

In this study, the two modeling paradigms were embedded in a canopy-scale model (ALEX) that was applied locally at selected sites using ground observations of meteorological and canopy variables. However, either canopy sub-model can potentially be used for mapping coupled fluxes of carbon and water at regional to continental scales if embedded in land surface schemes facilitating application to remote sensing data such as the two-source energy balance (TSEB) scheme (Anderson et al., 2008) and the Atmosphere-Land Exchange Inverse (ALEXI) model (Anderson et al., 2007).

6. Conclusion

'Bottom-up' (scaled-leaf) and 'top-down' (LUE-based) modeling paradigms for a coupled simulation of carbon and latent heat exchange were tested against eddy-covariance measurements over cropland, grassland and forest ecosystems across the continental U.S. Both canopy sub-models were able to reproduce observed magnitudes and variances of carbon and water vapor exchange on hourly and daily timescales with acceptable accuracy considering the simplicity of the ALEX modeling framework and the generality of the applied model parameterizations. Despite the simplicity of the LUE-based model it often performed better than the more detailed scaled-leaf model that has many species-specific model parameters that are a considerable challenge to specify with acceptable accuracy for applications over a variety of vegetative regimes. The use of a deactivation function in the temperature response functions for the Rubisco kinetic properties strongly influenced carbon flux simulations by the scaled-leaf model and resulted in large flux underestimations during early afternoon hours when air temperatures exceeded ~32 °C. Corresponding simulations by the LUE-based model, which currently does not incorporate effects of extreme temperatures on photosynthetic uptake, were in much better agreement with measurements. These findings suggest that the consideration of species-specific temperature acclimation response functions is critical for a successful implementation of scaled-leaf model parameterizations.

The incorporation of seasonal trends in photosynthetic efficiency (i.e., V_m^{25} and β_n) was needed to avoid bias in model simulations during leaf expansion and senescence at agricultural and deciduous forest sites. The simplistic methodology adopted here scales maximum Rubisco capacity and nominal LUE linearly with green leaf area index and is well suited to application over large regions as green leaf area index can be derived with reasonable accuracy from remote sensing.

Actual light-use efficiencies vary significantly in response to changing environmental conditions and the success of LUE-based modeling frameworks rely on their ability to realistically respond to changes in the light environment, atmospheric humidity, and CO_2 concentration. The described LUE-based model uses an effective LUE parameter that responds linearly to changes in the ratio of intercellular to ambient CO_2 concentration and the fraction of diffuse radiation. The incorporation of this C_i–LUE response into the analytical expression for the stomatal conductance was shown to be critical for tracking diurnal and day-to-day variations in CO_2 assimilation fluxes.

Acknowledgements

Funding for this research was provided by the USDA Agricultural Research Service Research Associate Program. The authors are indebted to the researchers responsible for the micrometeorological and surface flux measurements used in this analysis.

Appendix A

See Table A.1.

Appendix B

See Table B.1.

Table A.1
Photosynthesis and stomatal conductance equations of the scaled-leaf canopy.

Equation	Definition	No.
CO_2 and latent heat flux equations		
$A_{c,x} = \min\{A_{j,x}, A_{v,x}, A_{s,x}\} - R_{d,x}$	Net rate of CO_2 assimilation for sunlit and shaded canopy fractions	(A.1)
$A_{v,x} = \begin{cases} V_{m,x}\left(\frac{C_{i,x} - \Gamma_*}{C_{i,x} + K_c(1 + O/K_O)}\right) & \text{for } C_3 \\ V_{m,x} & \text{for } C_4 \end{cases}$	Rubisco limited rate of CO_2 assimilation for sunlit and shaded canopy fractions	(A.2)
$A_{j,x} = \begin{cases} J_x\left(\frac{C_{i,x} - \Gamma_*}{4(C_{i,x} + 2\Gamma_*)}\right) & \text{for } C_3 \\ \alpha_4 \mathrm{APAR}_x & \text{for } C_4 \end{cases}$	Light limited rate of CO_2 assimilation for sunlit and shaded canopy fractions	(A.3)
$J_x = \frac{\alpha_3 \mathrm{APAR}_x + J_{m,x} - \sqrt{(\alpha_3 \mathrm{APAR}_x + J_{m,x})^2 - 4\theta_j \alpha_3 \mathrm{APAR}_x J_{m,x}}}{2\theta_j}$	Irradiance dependence of electron transport for sunlit and shaded canopy fraction	(A.4)

Table A.1 (*Continued*)

Equation	Definition	No.
$A_{s,x} = \begin{cases} 0.5V_{m,x} & \text{for } C_3 \\ k_T C_{i,x}/10P & \text{for } C_4 \end{cases}$	Carbon compound export limited (C_3), or CO_2 limited (C_4) rate of photosynthesis for sunlit and shaded canopy fractions	(A.5)
$\left.\begin{array}{l}\theta_3 M^2 - M(A_{j,x} + A_{v,x}) + A_{j,x}A_{v,x} = 0 \\ \beta_3 A^2 - A(M + A_{s,x}) + MA_{s,x} = 0\end{array}\right\}$ for C_3 $\left.\begin{array}{l}\theta_4 M^2 - M(A_{j,x} + A_{v,x}) + A_{j,x}A_{v,x} = 0 \\ \beta_4 A^2 - A(M + A_{s,x}) + MA_{s,x} = 0\end{array}\right\}$ for C_4	Gross rate of CO_2 assimilation (A) is solved from nested quadratics to allow for colimitation between A_j, A_v and A_s	(A.6)
$C_{i,x} = C_{b,x} - 1.6R_{c,x}A_{c,x}$	Partial pressure of CO_2 in the intercellular spaces [μmol CO_2 mol^{-1} air]. The multiplier (1.6) is the ratio of diffusivities of CO_2 and water in air.	(A.7)
$C_{b,x} = C_a - 1.37R_{b,x}A_{c,x}$	Partial pressure of CO_2 in the leaf boundary layer [μmol CO_2 mol^{-1} air]. The multiplier (1.37) is the ratio of diffusivities of CO_2 and water vapor in the leaf boundary layer.	(A.8)
$\frac{1}{R_{c,x}} = b_{c,x} + m\frac{faw \times A_{c,x}RH_{b,x}}{C_{b,x}}$	Stomatal resistance of sunlit and shaded canopy fractions [mol m^{-2} s^{-1}]	(A.9)
$\rho_{vb} = \frac{R_{b,x}LE_{c,x}}{\lambda} + \rho_{vac}, \quad e_{b,x} = \rho_{vb}T_{K,x}\Re$ $RH_{b,x} = 1 - \frac{e*(T_{K,x}) - e_{b,x}}{e*(T_{K,x})}$	Relative humidity inside the leaf boundary layer for sunlit and shaded canopy fractions.	(A.10)
$LE_{c,x} = \frac{\lambda[e*(T_{K,x}) - e_{ac}]}{P(R_{c,x} + R_{b,x})}$	Latent heat flux for sunlit and shaded canopy fractions [W m^{-2}]	(A.11)
Temperature response functions		
$k_T = k \cdot 2^{(T_{K,x}-298)/10}$	Temperature dependence of the initial slope of photosynthetic CO_2 response (k)	(A.12)
$f(T_K) = k_{25}\exp\left[\frac{H_a(T_{K,x} - 298)}{298\Re T_{K,x}}\right]$ $k_{25} = \left\{K_c^{25}, K_o^{25}, \Gamma_*^{25}, R_{d,i}^{25}\right\}, \quad H_a = \{H_{a1}, H_{a2}, H_{a3}, H_{E6}\}$	Temperature dependences of K_c, K_o, $\Gamma*$ and R_d	(A.13)
$f(T_K) = k_{25}\exp\left[\frac{H_a(T_{K,x} - 298)}{298\Re T_{K,x}}\right]\frac{1 + \exp\left(\frac{298\Delta S - H_d}{298\Re}\right)}{1 + \exp\left(\frac{T_K\Delta S - H_d}{T_{K,x}\Re}\right)}$ $k_{25} = \left\{V_{m,i}^{25}, J_{m,i}^{25}\right\}, \quad H_a = \{H_{a5}, H_{a6}\}, \quad \Delta S = \{\Delta S_v, \Delta S_j\}$	Temperature dependences of V_m and J_m that account for the drop in activity at extreme temperatures	(A.14)
Leaf to canopy scaling functions		
$V_{m,1}^{25} = V_m^{25}L\left[\frac{1 - \exp(-k_n - k_bL\Omega)}{k_n + k_bL}\right]f_g f_{dry} \quad R_{d,1}^{25} = \frac{R_d^{25}}{V_m^{25}}V_{m,1}^{25}$	Photosynthetic Rubisco capacity and respiration (at 25 °C) of the sunlit canopy fraction	(A.15)
$V_{m,2}^{25} = V_m^{25}L\left[\frac{1 - \exp(-k_n)}{k_n} - \frac{1 - \exp(-k_n - k_bL\Omega)}{k_n + k_bL}\right]f_g f_{dry} \quad R_{d,2}^{25} = \frac{R_d^{25}}{V_m^{25}}V_{m,2}^{25}$	Photosynthetic Rubisco capacity and respiration (at 25 °C) of the shaded canopy fraction	(A.16)
$J_{m,1}^{25} = J_m^{25}L\left[\frac{1 - \exp(-k_d - k_bL\Omega)}{k_d + k_bL}\right]f_g f_{dry}$	Potential rate of electron transport (at 25 °C) of the sunlit canopy fraction	(A.17)
$J_{m,2}^{25} = J_m^{25}L\left[\frac{1 - \exp(-k_d)}{k_d} - \frac{1 - \exp(-k_d - k_bL\Omega)}{k_d + k_bL}\right]f_g f_{dry}$	Potential rate of electron transport (at 25 °C) of the shaded canopy fraction	(A.18)
$b_{c,1} = b\left[\frac{1 - \exp(-k_bL\Omega)}{k_b}\right]f_g f_{dry}$ $b_{c,2} = b\left[L - \frac{1 - \exp(-k_bL\Omega)}{k_b}\right]f_g f_{dry}$	The Ball and Berry offset for sunlit and shaded canopy fractions	(A.19)

where

x	=	$x = 1$ for sunlit and $x = 2$ for shaded canopy fraction
APAR	=	Absorbed photosynthetically active radiation [μmol m^{-2} s^{-1}]
P	=	Atmospheric pressure at surface [Pa] [0.1 μmol mol^{-1}]
e_{ac}	=	Actual vapor pressure in the canopy air space [Pa]
e_b	=	Actual vapor pressure in the leaf boundary layer [Pa]
$e^*(T_k)$	=	Saturation vapor pressure at leaf temperature [Pa]
faw	=	Fraction of available water in the root zone
f_g	=	Fraction of green vegetation
f_{dry}	=	Dry vegetation fraction
k_b	=	Extinction coefficient for direct-beam PAR
k_d	=	Extinction coefficient for diffuse PAR
R_b	=	Leaf boundary layer resistance for water vapor [s m^{-1}]
R_c	=	Stomatal resistance for water vapor [m s^{-1}]
T_K	=	Leaf temperature [K]
ρ_{vb}	=	Absolute humidity in the leaf boundary layer [kg m^{-3}]
ρ_{vac}	=	Absolute humidity in the canopy air space [kg m^{-3}]
R	=	Universal gas constant for water vapor [m^2 s^{-1} K^{-1}]
λ	=	Latent heat of evaporation [J kg^{-1}]

Table B.1
CO_2 assimilation and stomatal conductance equations of the LUE-based canopy sub-model.

Equation	Definition	No.
$LE_c = \frac{\lambda[e^*(T_K) - e_{ac}]}{P(R_c + R_b)}$	Canopy latent heat flux [W m^{-2}]	(B.1)
$LE_c = \lambda \frac{e^*(T_K)[1 - RH_b]}{PR_c}$	Canopy latent heat flux [W m^{-2}]	(B.2)
$A_c = \frac{C_i - C_a}{1.6R_c + 1.37R_b + R_a} = \frac{C_a - C_b}{1.37R_b + R_a}$	Canopy CO_2 assimilation (respiration not considered here but it is in Eq. (B.4))	(B.3)
$\frac{1}{R_c} = b_c + m\frac{faw \times A_c RH_b}{C_b}$ $b_c = b f_{dry} f_g L$	Bulk canopy stomatal resistance [mol m^{-2} s^{-1}]	(B.4)
$A_c = \beta(\gamma)\mathrm{APAR}$	Canopy CO_2 assimilation [μmol m^{-2} s^{-1}] as a function of LUE and APAR	(B.5)
$\gamma = \frac{C_i}{C_a}$	Ratio of intercellular to ambient CO_2 concentration (variable)	(B.6)
$\beta(\gamma) = \frac{\beta_n}{\gamma_n - \gamma_0}(\gamma - \gamma_0)$	Linear function modifying LUE in response to modeled C_i/C_a	(B.7)
$\beta_n^* = \begin{cases} \beta_n[1 + 2 \cdot 0.4(f_{dif} - 0.5)] & \text{for } C_3 \\ \beta_n[1 + 2 \cdot 0.15(f_{dif} - 0.5)] & \text{for } C_4 \end{cases}$	The effect of the fraction of diffuse lighting (f_{dif}) on the nominal LUE value	(B.8)

where; T_k, R_c, R_b, C_i, C_b, RH_b, b_c represent bulk canopy values. See Table A.1 and Table 2 for a description of parameters

References

Amthor, J.S., 1989. Respiration and Crop Productivity. Springer-Verlag, New York, 215 pp.

Anderson, M.C., Norman, J.M., Meyers, T.P., Diak, G.R., 2000. An analytical model for estimating canopy transpiration and carbon assimilation fluxes based on canopy light-use efficiency. Agric. For. Meteorol. 101, 265–289.

Anderson, M.C., Norman, J.M., Mecikalski, J.R., Otkin, J.A., Kustas, W.P., 2007. A climatological study of evapotranspiration and moisture stress across the continental United States based on thermal remote sensing: 1. Model formulation. J. Geophys. Res. 112, D10117, doi:10.1029/2006JD007506.

Anderson, M.C., Norman, J.M., Kustas, W.P., Houborg, R., Starks, P.J., Agam, N., 2008. A thermal-based remote sensing technique for routine mapping of land surface carbon, water and energy fluxes from field to regional scales. Remote Sens. Environ. 112, 4227–4241.

Baldocchi, D., 1994. An analytical solution for coupled leaf photosynthesis and stomatal counductance models. Tree Physiol. 14, 1069–1079.

Baldocchi, D., 1997. Measuring and modeling carbon dioxide and water vapour exchange over a temperate broad-leaved forest during the 1995 summer drought. Plant Cell Environ. 20, 1108–1122.

Baldocchi, D., 2003. Assessing the eddy covariance technique for evaluating carbon dioxide exchange rates of ecosystems: past, present and future. Global Change Biol. 9, 479–492.

Baldocchi, D., Wilson, K.B., 2001. Modeling CO_2 and water vapor exchange of a temperate broadleaved forest across hourly to decadal time scales. Ecol. Model. 142, 155–184.

Ball, J.T., Woodrow, I.E., Berry, J.A., 1987. A model predicting stomatal conductance and its contribution to the control of photosynthesis under different environmental conditions. In: Biggins, J. (Ed.), Progress in Photosynthesis Research. Nijhoff, Dodrecht, pp. 221–225.

Bernacchi, C.J., Singsaas, E.L., Pimentel, C., Portis, A.R., Long, S.P., 2001. Improved temperature response functions for models of Rubisco-limited photosynthesis. Plant Cell Environ. 24, 253–259.

Caemmerer von, S., Farquhar, G.D., 1981. Some relationships between the biochemistry of photosynthesis and the gas exchange of leaves. Planta 153, 376–387.

Caemmerer von, S., Evans, J.R., Hudson, G.S., Andrews, T.J., 1994. The kinetics of ribulose-1,5-bisphosphate carboxylase/oxygenase in vivo inferred from measurements of photosynthesis in leaves of transgenic tobacco. Planta 195, 88–97.

Campbell, G.S., Norman, J.M., 1998. An Introduction to Environmental Biophysics. Springer, New York.

Campbell, G.S., 1985. Soil physics with BASIC–Transport Models for Soil-Plant Systems. Elsevier, New York.

Chen, D.-X., Coughenour, M.B., Knapp, A.K., Owensby, C.E., 1994. Mathematical simulation of C4 grass photosynthesis in ambient and elevated CO_2. Ecol. Model. 73, 63–80.

Collatz, G.J., Ball, J.T., Grivet, C., Berry, J.A., 1991. Physiological and environmental regulation of stomatal conductance, photosynthesis and transpiration: a model that includes a laminar boundary layer. Agric. For. Meteorol. 54, 107–136.

Collatz, G.J., Ribas-Carbo, J., Berry, J.A., 1992. Coupled photosynthesis-stomatal conductance model for leaves of C4 plants. Aust. J. Plant Physiol. 19, 519–538.

Crafts-Brandner, S.J., Salvucci, M.E., 2002. Sensitivity of photosynthesis in a C4 plant, maize, to heat stress. Plant Physiol. 129, 1773–1780.

Creco, S., Baldocchi, D.D., 1996. Seasonal variations of CO_2 and water vapour exchange rates over a temperate deciduous forest. Global Change Biol. 2, 183–197.

Dai, Y., Dickenson, R.E., Wang, Y.-P., 2004. A two-big-leaf model for canopy temperature, photosynthesis, and stomatal conductance. J. Clim. 17, 2281–2299.

De Pury, D.G.G., Farquhar, G.D., 1997. Simple scaling of photosynthesis from leaves to canopies without the errors of big-leaf models. Plant Cell Environ. 20, 537–557.

Dickenson, R.E., Shaikh, M., Bryant, R., Graumlich, L., 1998. Interactive canopies for a climate model. J. Clim. 11, 2823–2836.

Dreyer, E., Le Roux, X., Montpied, P., Daudet, F.A., Masson, F., 2001. Temperature response of leaf photosynthetic capacity in seedlings from seven temperate tree species. Tree Physiol. 21, 223–232.

Edwards, N.T., Hanson, P.J., 1996. Stem respiration in a closed-canopy upland oak forest. Tree Physiol. 16, 433–439.

Ehleringer, J., Pearcy, R.W., 1983. Variation in quantum yield for CO_2 uptake among C3 and C4 plants. Plant Physiol. 73, 555–559.

Farquhar, G.D., von Caemmerer, S., Berry, J., 1980. A biochemical model of photosynthetic CO_2 assimilation in leaves of C3 species. Planta 149, 78–90.

Gilmanov, T.G., Tieszen, L.L., Wylie, B.K., Flanagan, L.B., Frank, A.B., Haferkamp, M.R., Meyers, T.P., Morgan, J.A., 2005. Integration of CO_2 flux and remotely-sensed data for primary production and ecosystem respiration analysis in the Northern Great Plains: potential for quantitative spatial extrapolation. Global Ecol. Biogeogr. 14, 271–292.

Gitelson, A.A., Vina, A., Verma, S.B., Rundquist, D.C., Arkebauer, T.J., Keydan, G., Leavitt, B., Ciganda, V., Burba, G.G., Suyker, A.E., 2006. Relationship between gross primary production and chlorophyll content in crops: Implications for the synoptic monitoring of vegetation productivity. J. Geophys. Res. 111, D08S11, doi:10.1029/2005JD006017.

Goudriaan, J., 1977. Crop Micrometeorology: A Simulation Study. Simulation Monographs, Wageningen.

Gower, S.T., Kucharik, C.J., Norman, J.M., 1999. Direct and indirect estimation of leaf area index, f_{APAR} and net primary production of terrestrial ecosystems. Remote Sens. Environ. 70, 29–51.

Gu, L., Baldocchi, D.D., Verma, S.B., Black, T.A., Vesala, T., Falge, E.M., Dowty, P.R., 2002. Advantages of diffuse radiation for terrestrial ecosystem productivity. J. Geophys. Res. 107 (D6), doi:10.1029/2001JD001242.

Gutschick, V.P., 1996. Physiological control of evapotranspiration by shrubs: scaling measurements from leaf to stand with the aid of comprehensive models. In: Barrow, J.R., McArthur, E.D., Sosebe, R.E., Tausch, R.J. (Eds.), Proceedings: Shrubland Ecosystem Dynamics in a Changing Environment, Las Cruces, NM.

Hansen, M., DeFries, R., Townshend, J.R.G., Sohlberg, R., 2000. Global land cover classification at 1 km resolution using a decision tree classifier. Int. J. Remote Sens. 21, 1331–1365.

Harley, P.C., Thomas, R.B., Reynolds, J.F., Strain, B.R., 1992. Modelling photosynthesis of cotton grown in elevated CO_2. Plant Cell Environ. 15, 271–282.

Haxeltine, A., Prentice, I.C., 1996. A general model for light use efficiency of primary production. Funct. Ecol. 10, 551–561.

Houborg, R.M., Soegaard, H., 2004. Regional simulation of ecosystem CO_2 and water vapor exchange for agricultural land using NOAA AVHRR and Terra MODIS satellite data. Application to Zealand, Denmark. Remote Sens. Environ. 93, 150–167.

Houborg, R., Anderson, M.C., Daughtry, C.T., 2009. Utility of an image-based canopy reflectance modeling tool for remote estimation of LAI and leaf chlorophyll content at the field scale. Remote Sens. Environ. 113, 259–274.
Kattge, J., Knorr, W., 2007. Temperature acclimation in a biochemical model of photosynthesis: a reanalysis of data from 36 species. Plant Cell Environ. 30, 1176–1190.
Kellomaki, S., Wang, K.-Y., 2000. Short-term environmental controls on carbon dioxide flux in a boreal coniferous forest: model computation compared with measurements by eddy covariance. Ecol. Model. 128, 63–88.
Kim, J., Verma, S.B., 1990. Carbon dioxide exchange in a temperate grassland ecosystem. Boundary-Layer Meteorol. 52, 135–149.
Kosugi, Y., Shibata, S., Kobashi, S., 2003. Parameterization of the CO_2 and H_20 gas exchange of several temperate deciduous broad-leaved trees at the leaf scale considering seasonal changes. Plant Cell Environ. 26, 285–301.
Kubien, D.S., Sage, R.F., 2004. Low-temperature photosynthetic performance of a C4 grass and a co-occuring C3 grass native to high latitudes. Plant Cell Environ. 27, 907–916.
Kuchari, C.J., Norman, J.M., Gower, S.T., 1999. Characterization of radiation regimes in nonrandom forest canopies: theory, measurements, and a simplified modeling approach. Tree Physiol. 19, 695–706.
Law, B.E., Waring, R.H., Anthoni, P.M., Aber, J., 2000. Measurements of gross and net ecosystem productivity and water vapour exchange of a Pinus ponderosa ecosystem, and an evaluation of two generalized models. Global Change Biol. 6, 155–168.
Lawrence, D.M., Slater, A.G., 2008. Incorporating organic soil into a global climate model. Clim. Dyn. 30, 145–160.
Leuning, R., 1990. Modelling stomatal behaviour and photosynthesis of Eucalyptus grandis. Aust. J. Plant Physiol. 17, 159–175.
Leuning, R., Kelliher, F.M., De Pury, D.G.G., Schulze, E.-D., 1995. Leaf nitrogen, photosynthesis, conductance and transpiration: scaling from leaves to canopies. Plant Cell Environ. 18, 1183–1200.
Leuning, R., Dunin, F.X., Wang, Y.-P., 1998. A two-leaf model for canopy conductance, photosynthesis and partitioning of available energy. II. Comparison with measurements. Agric. For. Meteorol. 91, 113–125.
Leuning, R., 2002. Temperature dependence of two parameters in a photosynthesis model. Plant Cell Environ. 25, 1205–1210.
Massad, R.-S., Tuzet, A., Bethenod, O., 2007. The effect of temperature on C4-type leaf photosynthesis parameters. Plant Cell Environ. 30, 1191–1204.
Massman, W., 1997. An analytical one-dimensional model of momentum transfer by vegetation of arbitrary structure. Bound.-Lay. Meteor. 83, 407–421.
Mayocchi, C.L., Bristow, K.L., 1995. Soil surface heat flux: some general questions and comments on measurements. Agric. For. Meteorol. 75, 43–50.
Medlyn, B.E., Dreyer, E., Ellsworth, D., Forstreuter, M., Harley, P.C., Kirschbaum, M.U.F., Roux, X.L.E., Montpied, P., Strassemeyer, J., Walcroft, A., Wang, K., Loustau, D., 2002. Temperature response of parameters of a biochemically based model of photosynthesis. II. A review of experimental data. Plant Cell Environ. 25, 1167–1179.
Moncrieff, J.B., Mahli, Y., Leuning, R., 1996. The propagation of errors in long term measurements of land atmosphere fluxes of carbon and water. Global Change Biol. 2, 231–240.
Nijs, I., Behaeghe, T., Impens, I., 1995. Leaf nitrogen content as a predictor of photosynthetic capacity in ambient and global change conditions. J. Biogeogr. 22, 177–183.
Norman, J.M., 1979. Modeling the complete crop canopy. In: Barfield, B.J., Gerber, J.F. (Eds.), Modification of the aerial environment of plants. ASAE, St. Joseph, MI.
Norman, J.M., Campbell, G., 1983. Application of a plantenvironment model to problems in irrigation. In: Hillel, D. (Ed.), Advances in Irrigation. Academic Press, New York, pp. 156–188.
Norman, J.M., Polley, W.R., 1989. Canopy photosynthesis. In: Briggs, W.R. (Ed.), Photosynthesis. Alan R. Liss, Inc., New York, pp. 227–241.
Norman, J.M., Arkebauer, T.J., 1991. Predicting canopy light-use efficiency from leaf characteristics. In: Modeling Plant and Soil Systems, Agronomy Mongraph No. 31, ASA-CSSA-SSSA, Madison, pp. 125–143.
Norman, J.M., Garcia, R., Verma, S.B., 1992. Soil surface CO_2 fluxes and the carbon budget of a grassland. J. Geophys. Res. 97, 18845–18853.
Potter, C., Klooster, S., Myneni, R., Genovese, V., Tan, P.-N., Kumar, V., 2003. Continental-scale comparisons of terrestrial carbon sinks estimated from satellite data and ecosystem modeling 1982–1998. Global Planet. Change 39, 201–213.
Prince, S.D., Goward, S.N., 1995. Global primary production: A remote sensing approach. J. Biogeogr. 22, 815–835.
Running, S.W., Hunt Jr., E.R., 1993. Generalization of a forest ecosystem model for other biomes, BIOME-BGC, and an application for global-scale models. In: Ehleringer, J.R., Field, C.B. (Eds.), Scaling Physiological Processes: Leaf to Globe. Academic Press, San Diego, CA, pp. 141–158.
Runyon, J., Waring, R.H., Goward, S.N., Welles, J.M., 1994. Environmental limits on net primary production and light-use efficiency across the Oregon transect. Ecol. Appl. 4, 226–237.
Ruimy, A., Saugier, B., Dedieu, G., 1994. Methodology for the estimation of terrestrial net primary production from remotely sensed data. J. Geophys. Res. 99, 5263–5283.
Ryan, M.G., Gower, S.T., Hubbard, R.M., Waring, R.H., Gholz, H.L., Cropper, W.P., Running, S.W., 1995. Woody tissue maintenance respiration of four conifers in contrasting climates. Oecologia 101, 133–140.
Sellers, P.J., Randall, D.A., Collatz, G.J., Berry, J.A., Field, C.B., Dazlich, D.A., Zhang, C., Collelo, G.D., Bounoua, L., 1996. A revised land surface parameterization (SIB2) for atmospheric GCMs. Part I: model formulation. J. Clim. 9, 676–705.
Soegaard, H., Nordstroem, C., 1999. Carbon dioxide exchange in a high-arctic fen estimated by eddy covariance measurements and modeling. Global Change Biol. 5, 547–562.
Spitters, C.J.T., 1986. Separating the diffuse and direct component of global radiation and its implications for modeling canopy photosynthesis. Part II. Calculation of canopy photosynthesis. Agric. For. Meteorol. 38, 231–242.
Turner, D.P., Urbanski, S., Bremer, D., Wofsy, S.C., Meyers, T., Gower, S.T., Gregory, M., 2003. A cross-biome comparison of daily light use efficiency for gross primary production. Global Change Biol. 9, 383–395.
Twine, T.E., Kustas, W.P., Norman, J.M., Cook, D.R., Houser, P.R., Meyers, T.P., Prueger, J.H., Starks, P.J., Wesely, M.L., 2000. Correcting eddy-covariance flux underestimates over a grassland. Agric. For. Meteorol. 103, 279–300.
Wagai, R., Brye, K.R., Gower, S.T., Norman, J.M., Bundy, L.G., 1998. Land use and environmental factors influencing soil surface CO_2 flux and microbial biomass in natural and managed ecoystems in southern Wisconsin. Soil Biol. Biochem. 30, 1501–1509.
Wang, Y.-P., Leuning, R., 1998. A two-leaf model for canopy conductance, photosynthesis and partitioning of available energy: I. Model description and comparison with a multi-layered model. Agric. For. Meteorol. 91, 89–111.
Wilson, K.B., Baldocchi, D.D., Hanson, P.J., 2000. Spatial and seasonal variability of photosynthetic parameters and their relationship to leaf nitrogen in a deciduous forest. Tree Physiol. 20, 565–578.
Wilson, K.B., Baldocchi, D.D., Hanson, P.J., 2001. Leaf age afffects the seasonal pattern of photosynthetic capacity and net ecosystem exchange of carbon in a deciduous forest. Plant Cell Environ. 24, 571–583.
Wilson, K.B., Goldstein, A., Falge, E., Aubinet, M., Baldocchi, D., Berbigier, P., Bernhofer, C., Ceulemans, R., Dolman, H., Field, C., Grelle, A., Ibrom, A., Law, B.E., Kowalski, A., Meyers, T., Moncrieff, J., Monson, R., Oechel, W., Tenhunen, J., Valentini, R., Verma, S., 2002. Energy balance closure at FLUXNET sites. Agric. For. Meteorol. 113, 223–243.
Wilson, T.B., Meyers, T.P., 2007. Determining vegetation indices from solar and photosynthetically active radiation fluxes. Agric. For. Meteorol. 144, 160–179.
Wofsy, S.C., Goulden, M.L., Munger, J.W., Fan, S.M., Bakwin, P.S., Daube, B.C., Bassow, S.L., Bazzaz, F.A., 1993. Net exchange of CO_2 in a mid-latitude forest. Science 260, 1314–1317.
Wohlfahrt, G., Bahn, M., Haubner, E., Horak, I., Michaeler, W., Rottmar, K., Tappeiner, U., Cernusca, A., 1999. Inter-specific variation of the biochemical limitation to photosynthesis and related leaf traits of 30 species from mountain grassland ecosystems under different land use. Plant Cell Environ. 22, 1281–1296.
Wong, S.C., Cowan, I.R., Farquhar, G.D., 1979. Stomatal conductance correlates with photosynthetic capacity. Nature 282, 424–426.
Wullschleger, S.D., 1993. Biochemical limitations to carbon assimilation in C_3 plants—a retrospective analysis of the A/C_i curves from 109 species. J. Exp. Bot. 44, 907–920.
Zhan, X., Kustas, W.P., 2001. A coupled model of land surface CO_2 and energy fluxes using remote sensing data. Agric. For. Meteorol. 107, 131–152.
Xu, L., Baldocchi, D.D., 2003. Seasonal trends in photosynthetic parameters and stomatal conductance of blue oak (*Quercus douglasii*) under prolonged summer drought and high temperature. Tree Physiol. 23, 865–877.